ISSN 0280-5316
ISRN LUTFD2/TFRT--5778--SE

Estimation of Side Wind Disturbances in Automotive Vehicles

Anders Widd

Department of Automatic Control
Lund University
November 2006

Department of Automatic Control
Lund Institute of Technology
Box 118
SE-221 00 Lund Sweden

Document name
MASTER THESIS

Date of issue
November 2006

Document Number
ISRNLUTFD2/TFRT--5778--SE

Author(s)
Anders Widd

Supervisor
Jens Kalkkuhl at DaimlerChrysler in Sindelfingen, Germany
Karl-Erik Årzén and Brad Schofield at Automatic Control in Lund.

Sponsoring organization

Title and subtitle
Estimation of Side Wind Disturbances in Automotive Vehicles (Skattning av sidvindsstörningar för fordon)

Abstract
This work is focused on a system which aims at estimating and attenuating side wind acting on a vehicle. The side wind disturbance is estimated using a disturbance observer. This thesis investigates the robustness towards sensor offset and parameter error. A few possibilities for reducing the effects of sensor offset are presented. A large part of the thesis is dedicated to on line identification of tyre parameters. Recursive Least Squares and Multiple Model Estimation are implemented in Matlab/Simulink and evaluated using measurement data. Both methods are found capable of distinguishing between ordinary tyres and winter tyres. A feedforward controller which uses the side wind estimate is also designed and evaluated in simulation.

Keywords

Classification system and/or index terms (if any)

Supplementary bibliographical information

ISSN and key title
0280-5316

ISBN

Language
English

Number of pages
70

Recipient's notes

Security classification

Acknowledgements

This thesis work was carried out at one of DaimlerChrysler's research facilities, REI/AR, in Sindelfingen, Germany between March and October 2006. I would like to thank the team in Sindelfingen for making my stay in Germany very pleasant and most of all Dr. Jens Kalkkuhl for his great supervision and support. I would also like to thank Prof. Karl-Erik Årzén at the Department of Automatic Control for giving me this opportunity and Brad Schofield who supervised from Lund.

Contents

1 Introduction **1**
- 1.1 Main Goals . . . 1
- 1.2 Thesis Outline . . . 2
- 1.3 Methods . . . 2
- 1.4 Notations . . . 3

2 Modeling **5**
- 2.1 Vehicle Model . . . 5
- 2.2 Modeling of Side Wind . . . 10
- 2.3 Modeling of Road Bank . . . 12
- 2.4 Second-Order Vehicle Model . . . 12
- 2.5 Modeling of Tyres . . . 13
- 2.6 Modeling of the Steering System . . . 15

3 Disturbance Observers **17**
- 3.1 Linear Observer . . . 17
- 3.2 Linear Disturbance Observer . . . 18
- 3.3 First-Order Disturbance Observer . . . 19
- 3.4 Robustness of the Side Wind Estimation . . . 21
  - 3.4.1 Sensitivity to Sensor Offset . . . 21
  - 3.4.2 A Moment-Based Estimate . . . 22
  - 3.4.3 Smoothing δ_{LR} . . . 24
  - 3.4.4 Estimation of Sensor Offset . . . 25
  - 3.4.5 Sensitivity to Parameter Error . . . 27

4 On Line Parameter Estimation **33**
- 4.1 Least Squares Estimation . . . 34
  - 4.1.1 Persistent Excitation . . . 34
  - 4.1.2 The Recursive Algorithm . . . 36
  - 4.1.3 LS1: Estimation of One Parameter . . . 37
  - 4.1.4 LS2: Estimation of Two Parameters . . . 37
  - 4.1.5 Introducing a Forgetting Factor in the SVD-test . . . 38
- 4.2 Multiple Model Estimation . . . 39

4.2.1 MME 1: Error Equation 41
4.2.2 MME 2: Multiple Model Observer 42
4.2.3 MME 3: Model Error 43
4.3 Implementation and Experimental Results 43
4.3.1 Comparison of the MME Strategies 44
4.3.2 The Role of the Forgetting Factor in LS2 45
4.3.3 Sensitivity to Sensor Offset 46
4.3.4 Identification of Ordinary and Winter Tyres 47
4.4 Aerodynamic Effects 49
4.4.1 Aerodynamic Drag 50
4.4.2 Aerodynamic Lift 52
4.4.3 Simulation Results 52

5 Closing the Loop **53**
5.1 The EPS-actuator 53
5.2 Controller Design 54
5.2.1 Feedforward Compensation 54
5.2.2 Tuning the Controller 56
5.2.3 Limiting the Controller 56

6 Conclusions and Future Work **59**
6.1 Conclusions 59
6.2 Future Work 59

Chapter 1

Introduction

Issues related to driver assistance and active safety are receiving a lot of attention in the automotive industry. They include measures taken to improve on the driver's experience and to help avoid accidents. An example of an active safety system is the anti-lock braking system (ABS) which reduces the risk of skidding during braking. Several systems for active safety and driver assistance are electronic and make use of sensors mounted on the vehicle. It is, however, important to keep the number of sensors as low as possible in order to minimize the production costs. The use of state observers is becoming widespread since they make it possible to extract more information from the available sensors. This thesis is a part of an ongoing project which aims at identifying and attenuating side wind acting on a vehicle.

The effects of side wind gusts are easily noted in several driving situations, for instance when passing a large truck or when entering a bridge. A heavy side wind gust can cause the vehicle to deviate from its track and into the meeting lane. When the gusts are modest, so that the driver can compensate for them, it will still be tiring to repeatedly perform compensating maneuvers which eventually makes the driver less responsive. By helping the driver to compensate for these disturbances, the safety is increased. Previous work has shown how pressure sensors on the vehicle may be used to measure the side wind in order to suppress the disturbance using feedforward control. The strategy currently used is known as a disturbance observer and only requires the sensors available in a vehicle equipped with an ESP-system.

1.1 Main Goals

The following points constitute the main goals of this master's project.

- Analyze the robustness to sensor offset and parameter error in the side wind estimation.
- Investigate possible ways of reducing the effects of sensor offset.
- Introduce on line identification of critical parameters to improve the side wind estimation.
- Design a controller which utilizes the side wind estimate.

1.2 Thesis Outline

The first part of this thesis deals with vehicle modeling. A simple vehicle model which covers the lateral dynamics during normal driving is derived in Chapter 2. The effects of side wind and road bank are also considered. A model of the steering system is introduced to facilitate the design of a controller later on.

The disturbance observer is derived in Chapter 3. An investigation of the robustness towards sensor offset and parameter error is performed. A few possibilities for reducing the effects of sensor offset are also presented.

Since the disturbance observer is found to be sensitive to parameter error, a large part of this thesis is dedicated to investigating the possibility of introducing on line identification of vehicle parameters. The investigation is focused on the use of Recursive Least Squares and Multiple Model Estimation. An introduction to both methods and experimental results are presented in Chapter 4.

A feedforward controller which uses the side wind estimate is designed and evaluated in Chapter 5.

1.3 Methods

Matlab and Simulink have been used extensively throughout this work. A simulation tool known as CASCaDE (Computer Aided Simulation of Car, Driver and Environment) was also used. It has been developed at Daimler-Chrysler and holds highly detailed models of several vehicles. It was used to simulate the controller when side wind was acting on the vehicle. Measurements made with test vehicles were used to evaluate the identification techniques.

1.4 Notations

Scalar signals and constants are written in small letters while matrices are written in capitals. Small, bold, letters denote vectors. An estimate of a signal or constant c is denoted $\hat{c}$ and the estimation error $c - \hat{c}$ is written $\tilde{c}$.

The relevant notations used in this thesis are presented in Table 1.1. Note that the cornering stiffnesses C_r and C_f generally will be presented in N/deg, although they are defined in N/rad.

Notation	Unit	Definition
α_f (α_r)	rad	Front (rear) tyre slip angle
a_y	m/s^2	Lateral acceleration
β	rad	Vehicle side slip angle
C_f (C_r)	N/rad	Cornering stiffness, front (rear) tyre
C_M	Nm/rad	Stiffness, steering rod
δ	rad	Steering angle
δ_{LR}	rad	Steering wheel angle
d_2	Nms/rad	Turning resistance, steering rod
e	m	Moment arm, side wind
g	m/s^2	Acceleration of gravity
i_L	-	Steering transmission ratio
J	kgm^2	Vehicle moment of inertia
J_2	kgm^2	Moment of inertia, lower part of the steering rod
L	m	Vehicle length
l_f (l_r)	m	Distance between front (rear) axle and center of gravity
m	kg	Vehicle mass
M_{LR}	Nm	Steering wheel torque
n_k	m	Distance between the wheel axle and the contact point between tyre and surface in the longitudinal direction
$\dot{\psi}$	rad/s	Yaw rate
T_s	s	Sample time
v_x	m/s	Vehicle longitudinal velocity
v_y	m/s	Vehicle lateral velocity

Table 1.1: Notations

Chapter 2

Modeling

The vehicle will be modeled using a one-track model (also known as bicycle model) which is a linear, second-order, model that provides reasonable fit under normal driving conditions. The dynamics of the steering system will also be modeled to facilitate the design of a feedforward controller. For further reading on modeling of vehicles, see [6], [4], [10].

2.1 Vehicle Model

Vehicle modeling requires the use of several coordinate systems. Two examples are the earth-fixed coordinate system (EFCS) and the vehicle-fixed coordinate system (VFCS), see Figure 2.1. The EFCS provides the environment in which the vehicle is moving. It is necessary in order to define the vehicle's velocity and acceleration, and the angle ψ, which is the angle between x' and x in Figure 2.1. The VFCS has its origin in the vehicle's center of gravity. The side slip angle, β, between x and the velocity vector, is defined in this coordinate system and given by $\beta = tan(v_y/v_x)$.

Figure 2.2 displays the VFCS and the lateral forces and torques acting on the vehicle during a turn. The lateral forces on the tyres must compensate for the force ma_y, which is due to the lateral acceleration a_y, and the torque $J\ddot{\psi}$, which is due to the vehicle's rotation around the center of gravity. The distances between the center of gravity and the front and rear axles are denoted l_f and l_r respectively. The velocity vector for each tyre, v_f and v_r, and the corresponding slip angles, α_f and α_r, are also displayed. A force equilibrium along the y-axis and a torque equilibrium around the z-axis (directed upwards in Figure 2.2) yield

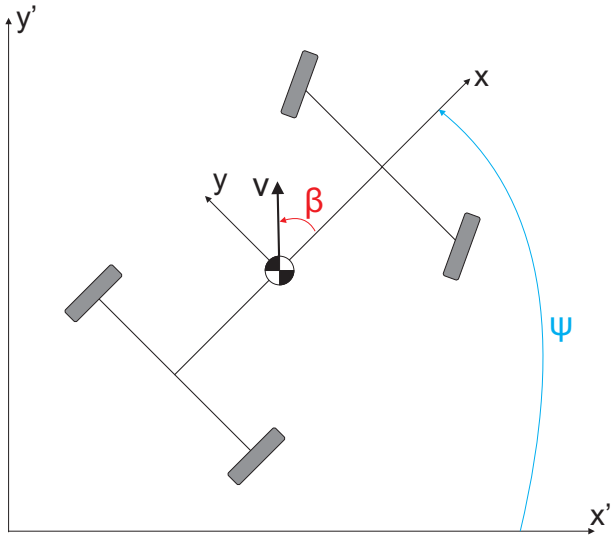

Figure 2.1: EFCS (x', y'), VFCS (x, y) and the side slip angle β.

$$ma_y = F_r + F_f cos(\delta) \tag{2.1}$$
$$J\ddot{\psi} = -l_r F_r + l_f F_f cos(\delta) \tag{2.2}$$

Under the assumption that there is a linear relation between the slip angles and the lateral forces on the tyres, the tyre forces may be expressed using the cornering stiffnesses, C_f and C_r, in the following way.

$$F_f = C_f \alpha_f \tag{2.3}$$
$$F_r = C_r \alpha_r \tag{2.4}$$

In reality, tyre forces are highly non-linear, but since the model is to be used under normal driving conditions, a linear approximation is possible, see Section 2.5. By inserting (2.3) and (2.4), Equations (2.1) and (2.2) become

$$ma_y = C_r \alpha_r + C_f \alpha_f cos(\delta) \tag{2.5}$$
$$J\ddot{\psi} = -l_r C_r \alpha_r + l_f C_f \alpha_f cos(\delta) \tag{2.6}$$

The next step is to express a_y in its components. If the vehicle is approximated by a rigid body, the acceleration of the center of gravity, a_{CoG}, is

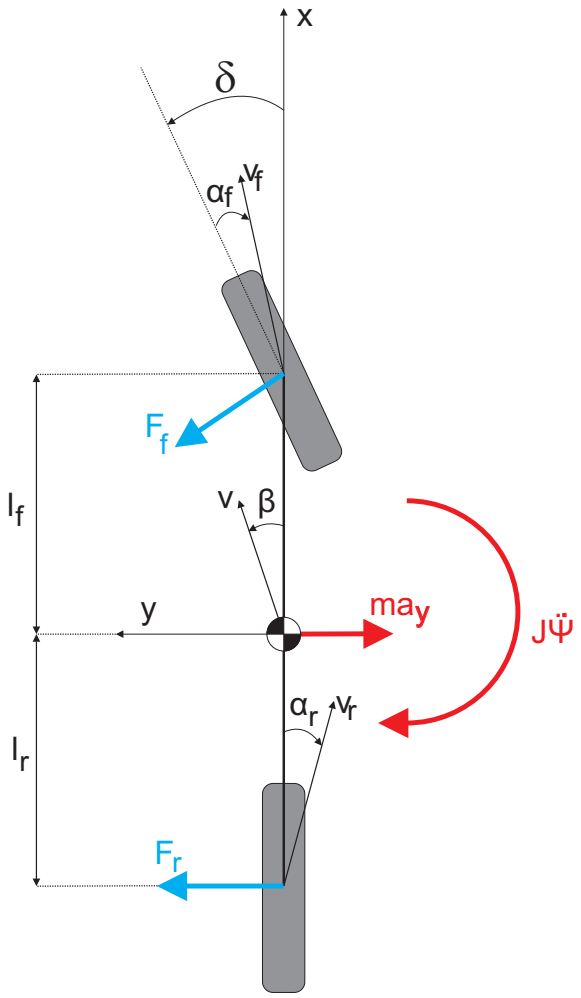

Figure 2.2: The one-track vehicle model and the relevant forces and torques.

$$\mathbf{a}_{CoG} = \dot{\mathbf{v}}_{CoG} + \omega \times \mathbf{v}_{CoG} = \begin{pmatrix} \dot{v}_x \\ \dot{v}_y \\ 0 \end{pmatrix} + \begin{pmatrix} 0 \\ 0 \\ \dot{\psi} \end{pmatrix} \times \begin{pmatrix} v_x \\ v_y \\ 0 \end{pmatrix} = \begin{pmatrix} \dot{v}_x - v_y\dot{\psi} \\ \dot{v}_y + v_x\dot{\psi} \\ 0 \end{pmatrix} \tag{2.7}$$

where ω is a vector containing the angular velocity of the center of gravity. It is assumed that only planar motion occurs, meaning that ω only has a component in the z-direction and that $v_z = \dot{v}_z = 0$. This yields that

$$a_y = \dot{v}_y + v_x\dot{\psi} \tag{2.8}$$

To rewrite the model further, the slip angles may be expressed in other

variables. The velocities of the tyres may be expressed in VFCS as follows

$$\mathbf{v}_r = (v_r \cos(\alpha_r), -v_r \sin(\alpha_r), 0)^T \quad (2.9)$$
$$\mathbf{v}_f = (v_f \cos(\alpha_f), v_f \sin(\alpha_f), 0)^T \quad (2.10)$$

Under the assumption of small angles, the approximations $\cos(\delta) \approx 1$ and $\sin(\delta) \approx \delta$ may be used, yielding the following approximate equalities.

$$\mathbf{v}_r \approx (v_r, -v_r \alpha_r, 0)^T \quad (2.11)$$
$$\mathbf{v}_f \approx (v_f, v_f \alpha_f, 0)^T \quad (2.12)$$

Under the assumption of a rigid body, the velocities can also be expressed through $\mathbf{v}_r = \mathbf{v}_{CoG} + \omega \times \mathbf{r}_r$ and $\mathbf{v}_f = \mathbf{v}_{CoG} + \omega \times \mathbf{r}_f$, where $\mathbf{r}_r$ and $\mathbf{r}_f$ are the distances from the center of gravity to the rear wheel and front wheel respectively.

$$\mathbf{v}_r = (v_x, v_y, 0)^T + (0, 0, \dot{\psi})^T \times (-l_r, 0, 0)^T = (v_x, v_y - l_r\dot{\psi}, 0)^T \quad (2.13)$$
$$\mathbf{v}_f = (v_x, v_y, 0)^T + (0, 0, \dot{\psi})^T \times (l_f, 0, 0)^T = (v_x, v_x + l_f\dot{\psi}, 0)^T \quad (2.14)$$

Setting (2.11) equal to (2.13) and (2.12) equal to (2.14) the following expression for α_f and α_r are obtained.

$$\alpha_r = -\beta + \frac{l_r\dot{\psi}}{v} \quad (2.15)$$
$$\alpha_f = -\beta - \frac{l_f\dot{\psi}}{v} + \delta \quad (2.16)$$

If it is assumed that $v_y << v_x$, the approximations $\beta = \tan\frac{v_y}{v_x} \approx \frac{v_y}{v_x}$ and $v \approx v_x$ hold. Inserting Equations (2.8), (2.15) and (2.16) into (2.5) and (2.6) yields the following equations.

$$m\dot{v}_y = C_r\frac{l_r\dot{\psi} - v_y}{v_x} + C_f\left(\delta - \frac{l_f\dot{\psi} + v_y}{v_x}\right) \quad (2.17)$$
$$J\ddot{\psi} = l_f C_f\left(\delta - \frac{l_f\dot{\psi} + v_y}{v_x}\right) - l_r C_r\frac{l_r\dot{\psi} - v_y}{v_x} \quad (2.18)$$

Introducing the notations

$$S_f = C_f\left(\delta + \frac{-v_y - l_f\dot{\psi}}{v_x}\right) \tag{2.19}$$

$$S_r = C_r\frac{l_r\dot{\psi} - v_y}{v_x} \tag{2.20}$$

simplifies the equations of motion to

$$\dot{v}_y = -\dot{\psi}v_x + \frac{S_f + S_r}{m} \tag{2.21}$$

$$\ddot{\psi} = \frac{l_f S_f - l_r S_r}{J} \tag{2.22}$$

These two equations constitute the second-order one-track model. For verification purposes, the steering angle and velocity of a test drive with a real vehicle were used as inputs. The calculated yaw rate and lateral acceleration were then compared to those of the real vehicle. The results are presented in Figure 2.3. The most noticeable difference between the model and the real vehicle is the transients which occur in both $\dot{\psi}$ and a_y. To a large extent, these are due to unmodeled dynamics in the vehicle but the differences are still fairly small. The model captures the lateral dynamics of the vehicle under normal driving conditions.

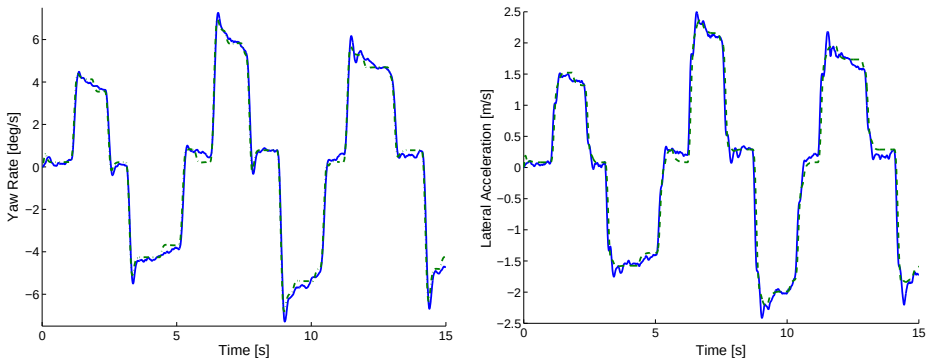

(a) Yaw rate $\dot{\psi}$. (b) Lateral acceleration a_y.

Figure 2.3: The output of the one-track model (green- -) and the measured output (blue–).

When deriving this model, some assumptions were needed. A few of these are summarized below.

- Planar motion, only rotational and translational movement in the xy-plane is considered.
- $v_x >> v_y$.
- Small angles δ, α_r and α_f.
- Linear relation between lateral forces and slip angles.

2.2 Modeling of Side Wind

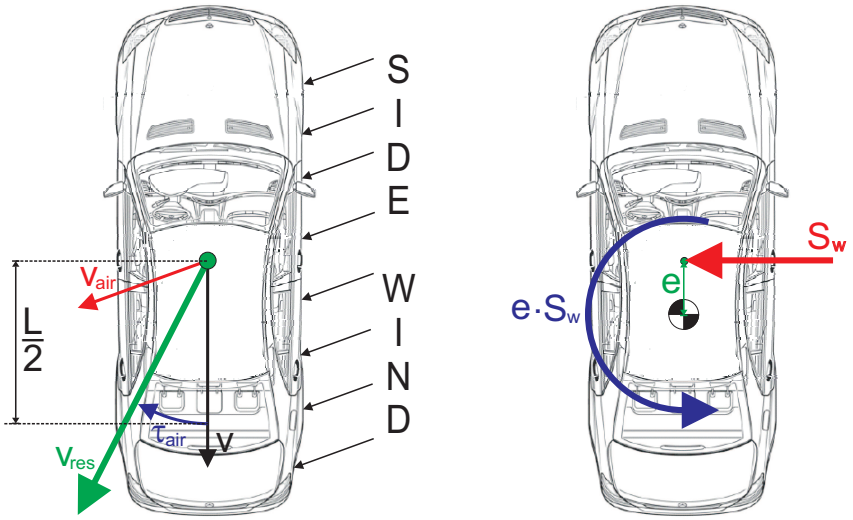

(a) The resulting velocity v_{res} and the angle of attack τ_w.

(b) Resulting force S_w and the moment arm e.

Figure 2.4: Two ways of modeling side wind.

The air resistance acting on a vehicle yields forces $F_{w,x}$, $F_{w,y}$ and $F_{w,z}$ proportional to the velocity squared, according to the following equation, where $\boldsymbol{v}^2$ indicate the vector product $\boldsymbol{v}^T\boldsymbol{v}$, [4].

$$F_{w,\iota} = \frac{\rho_{air}}{2} c_{air,\iota}(\tau_{air}) A_{air} \boldsymbol{v}^2, \quad \iota = x, y, z \tag{2.23}$$

The density of air is denoted ρ_{air} and A_{air} is the area of the vehicles front surface. The coefficients $c_{air,\iota}$ are functions of the angle τ_{air} between the velocity $\boldsymbol{v}$ and the direction in which the vehicle is pointing. The moments $M_{w,x}$, $M_{w,y}$ and $M_{w,z}$ around each axis is given by a similar expression.

$$M_{w,\iota} = \frac{\rho_{air}}{2} c_{air,\iota\iota}(\tau_{air}) A_{air} \boldsymbol{v}^2 L, \quad \iota = x, y, z \tag{2.24}$$

Note that aerodynamic forces usually are calculated in a coordinate system situated in the center of the vehicle, which does not always coincide with the center of gravity.

The force generated by side wind can be calculated by adding the wind velocity $\boldsymbol{v}_{air}$ to the velocity corresponding to the vehicles movement, $\boldsymbol{v}$, to form the resulting velocity vector $\boldsymbol{v}_{res}$ as depicted in Figure 2.4 (a). The lateral force $F_{w,y}$ and the moment $M_{w,z}$ around the vertical axis are then given by

$$\begin{aligned} F_{w,y} &= \tfrac{\rho_{air}}{2} c_{air,y}(\tau_{air}) A_{air} \boldsymbol{v}_{res}^2 \\ M_{w,z} &= \tfrac{\rho_{air}}{2} c_{air,zz}(\tau_{air}) A_{air} \boldsymbol{v}_{res}^2 L \end{aligned}$$

For the side wind compensation, it is not necessary to obtain the actual wind direction and velocity. It is therefore assumed that the wind generates a force $S_w = F_{w,y}$ in the lateral direction which attacks the vehicle in a point at a distance e from the center of gravity, generating a moment eS_w as depicted in Figure 2.4 (b). This simplifies the modeling but still captures the effects on the lateral dynamics. To calculate e, $M_{w,z}$ is expressed in S_w according to

$$M_{w,z} = \frac{c_{air,zz}(\tau_{air})}{c_{air,y}(\tau_{air})} L S_w$$

Since the aerodynamic center is situated in the center of the vehicle, the distance between this point and the center of gravity is $L/2 - l_r$. The moment eS_w around the vertical axis in the center of gravity is then given by

$$eS_w = \left(\frac{L}{2} - l_r \right) S_w + M_{w,z} = \left(\frac{c_{air,zz}(\tau_{air})}{c_{air,y}(\tau_{air})} - \frac{l_r}{L} + \frac{1}{2} \right) L S_w$$

which gives the following expression for e

$$e = \left(\frac{c_{air,zz}(\tau_{air})}{c_{air,y}(\tau_{air})} - \frac{l_r}{L} + \frac{1}{2} \right) L$$

In the modeling, e will be assumed to be constant. The approximation holds in most cases since the angle τ_{air} is rather small at high speeds.

The force S_w and moment eS_w are included in the one-track model by adding the force to (2.21) and the moment to (2.22), which results in the following equations of motion.

$$\dot{v}_y = -\dot{\psi}v_x + \frac{S_f + S_r}{m} + \frac{S_w}{m} \tag{2.25}$$

$$\ddot{\psi} = \frac{l_f S_f - l_r S_r}{J} + \frac{eS_w}{J} \tag{2.26}$$

2.3 Modeling of Road Bank

Another disturbance which commonly affects vehicles is road bank. The weight of the vehicle then has a component in the lateral direction, according to Figure 2.5. Under the assumption of small angles the approximation $mg\sin(\Phi_R) \approx mg\Phi_R$ holds. The force does not influence the yaw rate directly, but it affects the lateral acceleration. Equation (2.25) then becomes

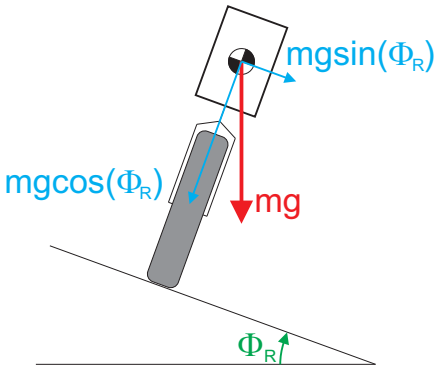

Figure 2.5: The additional force $mg\sin(\Phi_R)$ in the lateral direction when the road is banked.

$$\dot{v}_y = -\dot{\psi}v_x + \frac{S_f + S_r}{m} - g\Phi_R + \frac{S_w}{m} \tag{2.27}$$

2.4 Second-Order Vehicle Model

The equations of motion for the one-track model with the disturbances S_w and Φ_R added, (2.26) and (2.27), are repeated below.

$$\dot{v}_y = -\dot{\psi}v_x + \frac{S_f + S_r + S_w}{m} - g\Phi_R \tag{2.28}$$

$$\ddot{\psi} = \frac{l_f S_f - l_r S_r + eS_w}{J} \tag{2.29}$$

The system may also be presented on the state space form of (2.31) by choosing

$$\mathbf{x} = (v_y \;\; \dot{\psi})^T, \quad u = \delta, \quad \mathbf{f} = (\Phi_R \;\; S_w)^T, \quad \mathbf{y} = (a_y \;\; \dot{\psi})^T \tag{2.30}$$

$$\begin{aligned} \dot{\mathbf{x}} &= A\mathbf{x} + Bu + G\mathbf{f} \\ \mathbf{y} &= C\mathbf{x} + Du + H\mathbf{f} \end{aligned} \tag{2.31}$$

which yields the following matrices

$$A = \begin{pmatrix} -\frac{\sigma}{mv_x} & \frac{\rho}{mv_x} - v_x \\ \frac{\rho}{Jv_x} & -\frac{\kappa}{Jv_x} \end{pmatrix} \quad B = \begin{pmatrix} \frac{C_f}{m} \\ \frac{l_f C_f}{J} \end{pmatrix} \quad C = \begin{pmatrix} -\frac{\sigma}{mv_x} & \frac{\rho}{mv_x} \\ 0 & 1 \end{pmatrix}$$

$$D = \begin{pmatrix} \frac{C_f}{m} \\ 0 \end{pmatrix} \qquad G = \begin{pmatrix} -g & \frac{1}{m} \\ 0 & \frac{e}{J} \end{pmatrix} \qquad H = \begin{pmatrix} 0 & \frac{1}{m} \\ 0 & 0 \end{pmatrix} \tag{2.32}$$

where the notations ρ, σ and κ are defined as

$$\rho = l_r C_r - l_f C_f \tag{2.33}$$

$$\sigma = C_f + C_r \tag{2.34}$$

$$\kappa = l_f^2 C_f + l_r^2 C_r \tag{2.35}$$

The system may also be presented on the following form.

$$\begin{aligned} \dot{\mathbf{x}} &= A\mathbf{x} + B\mathbf{u} \\ \mathbf{y} &= C\mathbf{x} + D\mathbf{u} \end{aligned} \tag{2.36}$$

To do this, the output vector is set to $\mathbf{y} = (a_y \;\; \dot{\psi})^T$ and the input vector to $\mathbf{u} = (\delta \;\; \Phi_R \;\; S_w)^T$ which yields the following matrices, expressed in those of (2.32). The subscript $_2$ indicate that they constitute the second-order vehicle model.

$$A_2 = A \quad B_2 = \begin{pmatrix} B & G \end{pmatrix} \quad C_2 = C \quad D_2 = \begin{pmatrix} D & H \end{pmatrix} \tag{2.37}$$

2.5 Modeling of Tyres

To simplify matters, this section will discuss modeling of the front tyres only, although the results apply to the rear tyres also.

When driving and braking a vehicle, forces occur between the tyre and the road due to the relative velocity between them. As a measure of the relative velocity, longitudinal and lateral slip, denoted λ_l and λ_f, are introduced.

$$\lambda_l = \frac{\omega_w r_w cos(\alpha_f) - v_f}{\omega_w r_w} \approx \frac{\omega_w r_w - v_f}{\omega_w r_w} \quad (2.38)$$

$$\lambda_f = tan(\alpha_f) \approx \alpha_f \quad (2.39)$$

In the equations above v_f is the wheel velocity, ω_w is the wheel's angular velocity, r_w is the wheel radius and α_f is the slip angle, as defined in Figure 2.2. The slip angles are assumed to be small during normal driving. Lateral forces only occur when $\alpha_f \neq 0$, which gives rise to lateral slip λ_f. The slip angle and the directions in which slip occurs are depicted in Figure 2.6 (a).

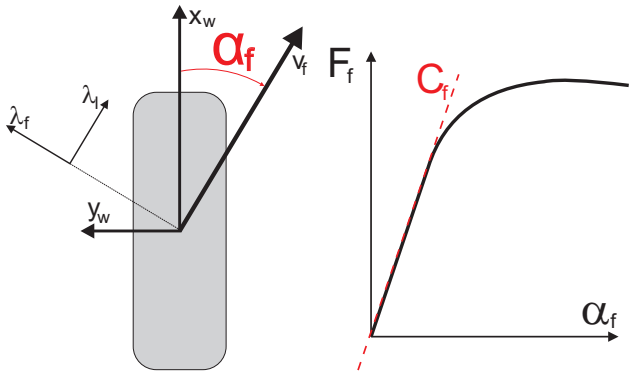

(a) Slip angle. (b) Cornering stiffness, C_f.

Figure 2.6: (a) Definition of slip angles and the directions in which slip occurs. (b) The cornering stiffness is the initial slope of the curve.

The quotient between the force between tyre and road, and the vertical force acting on the wheel, $F_{z,f}$, is called *friction coefficient* and denoted μ. There are several models for calculating μ, one of them is the Burckhardt approach below.

$$\mu(\lambda) = c_1(1 - e^{-c_2\lambda}) - c_3\lambda$$

where $\lambda = \sqrt{\lambda_l^2 + \lambda_f^2}$. The lateral and longitudinal coefficients are given by

$$\mu_l = \mu\frac{\lambda_l}{\lambda} \quad \mu_f = \mu k_f \frac{\lambda_f}{\lambda}$$

The longitudinal and lateral forces are then given by

$$F_l = \mu_l F_{z,f} \quad (2.40)$$

$$F_f = \mu_f F_{z,f} \quad (2.41)$$

Figure 2.6 (b) shows the typical shape of F_f as a function of α_f. The relationship between F_l and λ_l is similar. The cornering stiffness C_f and the longitudinal stiffness C_l are defined as the initial slope of these curves. A linearization around $\lambda_l = \lambda_f = 0$ yields

$$F_l = \frac{\partial}{\partial \lambda_l}\Big(\mu_l F_{z,f}\Big)\Big|_{\lambda_l=\lambda_f=0} \lambda_l = C_l \lambda_l \approx C_l \lambda \tag{2.42}$$

$$F_f = \frac{\partial}{\partial \lambda_f}\Big(\mu_f F_{z,f}\Big)\Big|_{\lambda_l=\lambda_s=0} \lambda_f = C_f \lambda_f \approx C_f \alpha_f \tag{2.43}$$

In the following, C_f and C_r, α_f and α_r will denote the cornering stiffness and slip angle of the front and rear tyre respectively.

2.6 Modeling of the Steering System

The steering is constructed as in Figure 2.7 where C_M is the stiffness of the steering rod, d_2 is the turning resistance and J_2 is the moment of inertia of the lower part of the steering rod. The steering wheel angle δ_{LR} is set by the driver and is the translated into steering angle δ. The steering rod is modeled with a spring. The torque M_{LR} is applied via an electric motor while the turning velocity, $\dot{\delta}$, is measured. This is known as Electronic Power Steering (EPS). The force acting on the front wheel yields a torque $n_k S_f$ due to the caster which places the contact point between tyre and surface behind the wheel axis.

A torque equilibrium around the steering rod yields

$$J_2\ddot{\delta} + d_2\dot{\delta} + C_M i_L(\delta - \frac{\delta_{LR}}{i_L}) = M_{LR} i_L - n_k C_f(\delta - \frac{v_y}{v_x} - \frac{l_f\dot{\psi}}{v_x}) \tag{2.44}$$

This model will later be used to design a feedforward controller that utilizes a moment actuator on the steering rod.

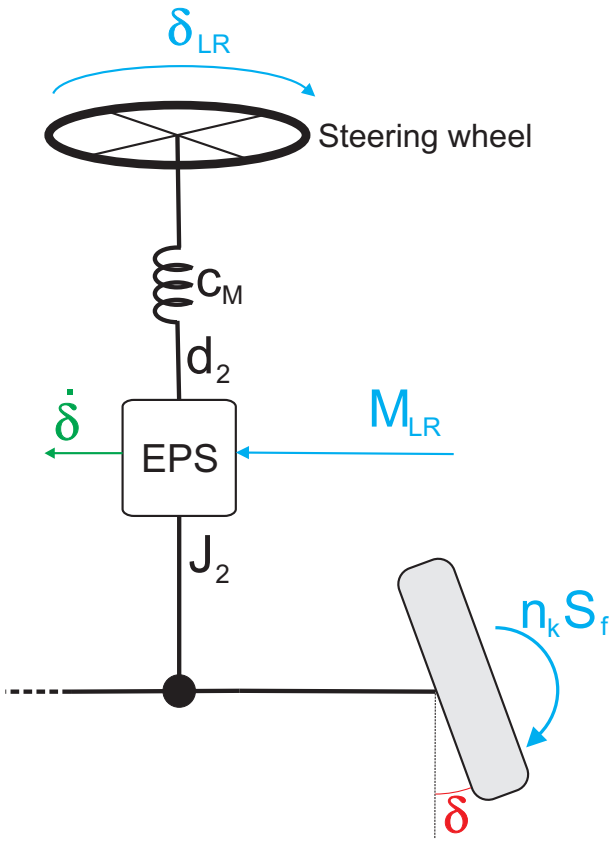

Figure 2.7: Model of the steering system.

Chapter 3

Disturbance Observers

An observer is typically used to estimate the states of a system when no, or poor, measurements are available. The method works for both single-input-single-output (SISO) and multiple-input-multiple-output (MIMO) systems. The estimated states may in turn be used for controlling the system. However, the structure of the observer may also be used to estimate disturbances acting on the system, which will be performed in the following.

3.1 Linear Observer

Consider the linear MIMO system below, where $A \in \mathbb{R}^{n\times n}$, $B \in \mathbb{R}^{n\times m}$ and $C \in \mathbb{R}^{p\times n}$. It is assumed that the system is observable, meaning that the observability matrix, $W_o = \begin{pmatrix} C & CA & \dots & CA^{n-1} \end{pmatrix}^T$ has full rank.

$$\begin{aligned} \dot{\boldsymbol{x}} &= A\boldsymbol{x} + B\boldsymbol{u} \\ \boldsymbol{y} &= C\boldsymbol{x} \end{aligned} \tag{3.1}$$

It is assumed that $\boldsymbol{y}$ is measurable while $\boldsymbol{x}$ is not. An observer for this system is given as follows, with $K \in \mathbb{R}^{n\times p}$.

$$\begin{aligned} \dot{\hat{\boldsymbol{x}}} &= A\hat{\boldsymbol{x}} + B\boldsymbol{u} + K(\boldsymbol{y} - \hat{\boldsymbol{y}}) \\ \hat{\boldsymbol{y}} &= C\hat{\boldsymbol{x}} \end{aligned} \tag{3.2}$$

The state estimation error $\tilde{\boldsymbol{x}} = \boldsymbol{x} - \hat{\boldsymbol{x}}$ then has the dynamics $\dot{\tilde{\boldsymbol{x}}} = (A - KC)\tilde{\boldsymbol{x}}$. As long as the matrix K is chosen so that $A - KC$ is Hurwitz, the state estimation error tends to zero. However, an umodeled disturbance acting on the input of the system will generate an error in the estimate. In the following section it will be demonstrated how this may be exploited in order

to estimate the disturbance. For further reading on disturbance observers, see [2] for a good presentation of the linear case or [3] which also deals with nonlinear disturbance observers.

3.2 Linear Disturbance Observer

Assume that a disturbance $\boldsymbol{f} \in \mathbb{R}^{m\times 1}$ enters the system according to (3.3), where the matrices A, B and C have the same dimensions as in the previous section.

$$\begin{aligned} \dot{\boldsymbol{x}} &= A\boldsymbol{x} + B(\boldsymbol{u} + \boldsymbol{f}) \\ \boldsymbol{y} &= C\boldsymbol{x} \end{aligned} \tag{3.3}$$

A discretization yields

$$\begin{aligned} \boldsymbol{x}[k+1] &= \Phi_d \boldsymbol{x}[k] + \Gamma_d(\boldsymbol{u}[k] + \boldsymbol{f}[k]) \\ \boldsymbol{y}[k] &= C\boldsymbol{x}[k] \end{aligned} \tag{3.4}$$

where

$$\Phi_d = e^{ATs}, \quad \Gamma_d = \int_0^{T_s} e^{A\tau} B d\tau$$

An observer is designed without taking the disturbance into account.

$$\begin{aligned} \hat{\boldsymbol{x}}[k+1] &= \Phi_d \hat{\boldsymbol{x}}[k] + \Gamma_d \boldsymbol{u}[k] + K(\boldsymbol{y}[k] - \hat{\boldsymbol{y}}[k]) \\ \hat{\boldsymbol{y}}[k] &= C\hat{\boldsymbol{x}}[k] \end{aligned} \tag{3.5}$$

The dynamics of the estimation error is

$$\tilde{\boldsymbol{x}}[k+1] = (\Phi_d - KC)\tilde{\boldsymbol{x}}[k] + \Gamma_d \boldsymbol{f}[k] \tag{3.6}$$

$$\tilde{\boldsymbol{y}}[k] = C\tilde{\boldsymbol{x}}[k] \tag{3.7}$$

Choosing K so that the poles of $\Phi_d - KC$ lie in the unit circle makes the estimation error bounded-input-bounded-output stable but it does not necessarily tend to zero. To estimate $\boldsymbol{f}$ it is necessary to obtain an expression containing only $\boldsymbol{f}$ and $\tilde{\boldsymbol{y}}$, since $\tilde{\boldsymbol{x}}$ is not measurable. When C^{-1} exists, this is possible through

$$\tilde{\boldsymbol{y}}[k+1] - \left(C\Phi_d C^{-1} - CK\right)\tilde{\boldsymbol{y}}[k] = C\Gamma_d \boldsymbol{f}[k] \tag{3.8}$$

which is easily verified by direct calculation and using (3.6) - (3.7). When $(C\Gamma_d)^{-1}$ exists, an estimate of $\boldsymbol{f}$ is

$$\hat{\boldsymbol{f}}[k] = (C\Gamma_d)^{-1}\left(\tilde{\boldsymbol{y}}[k+1] - \left(C\Phi_d C^{-1} - CK\right)\tilde{\boldsymbol{y}}[k]\right) \tag{3.9}$$

In the SISO-case, $C\Gamma_d$ is scalar, which makes estimation possible as long as $C\Gamma_d \neq 0$.

A problem with this estimate is that it uses $\tilde{y}[k+1]$, which is not known at time k. The approximation

$$\hat{\boldsymbol{f}}[k] \approx \hat{\boldsymbol{f}}[k-1] = (C\Gamma_d)^{-1}\left(\tilde{\boldsymbol{y}}[k] - \left(C\Phi_d C^{-1} - CK\right)\tilde{\boldsymbol{y}}[k-1]\right) \tag{3.10}$$

may therefore be used. Delaying the estimate of $\boldsymbol{f}$ by one sample produces the estimation error $\tilde{\boldsymbol{f}}[k] = \boldsymbol{f}[k] - \boldsymbol{f}[k-1]$. This error will only be zero when the disturbance is constant, so that $\boldsymbol{f}[k] = \boldsymbol{f}[k-1]$. When the disturbance is changing between samples, the error will be smaller for a given change in the disturbance the shorter the sample time is.

3.3 First-Order Disturbance Observer

A first-order disturbance observer which only considers the yaw rate will now be presented. Since only side wind is to be estimated, the road bank Φ_R is set to zero. By using the expression $a_y = \dot{v}_y + \dot{\psi} v_x$, which was derived in Chapter 2, the equation for lateral velocity, (2.28), takes the following form.

$$ma_y = S_f + S_r + S_w \tag{3.11}$$

Solving for S_f and inserting it into (2.29) yields

$$\ddot{\psi} = \frac{l_f m a_y}{Jzz} - \frac{L}{Jzz} S_r + \frac{e - l_f}{Jzz} S_w \tag{3.12}$$

By putting the expression for S_f derived from (3.11) equal to (2.19) the following equation is obtained

$$ma_y - S_r - S_w = C_f \delta - C_f \frac{v_y}{v_x} - \frac{l_f C_f}{v_x}\dot{\psi}$$

Inserting the expression for S_r, (2.20), and solving for $\frac{v_y}{v_x}$ yields

$$\frac{v_y}{v_x} = \frac{1}{\sigma}\left(\frac{\rho}{v_x}\dot{\psi} + C_f\delta + S_w - ma_y\right) \tag{3.13}$$

By inserting this expression into (2.20) an expression for S_r which does not contain v_y is obtained. This may in turn be inserted into (3.12), which gives the following expression.

$$\ddot{\psi} = -\frac{L^2C_fC_r}{J\sigma v_x}\dot{\psi} - \frac{m\rho}{J\sigma}a_y + \frac{LC_fC_r}{J\sigma}\delta + \frac{1}{J}\left(e + \frac{\rho}{\sigma}\right)S_w \tag{3.14}$$

By introducing the notations

$$A_{obs} = -\frac{L^2C_fC_r}{J\sigma v_x} \tag{3.15}$$

$$u = \frac{LC_fC_r}{J\sigma}\delta - \frac{m\rho}{J\sigma}a_y \tag{3.16}$$

$$f = \frac{1}{J}\left(e + \frac{\rho}{\sigma}\right)S_w \tag{3.17}$$

the system may be written on the following form

$$\ddot{\psi} = A_{obs}\dot{\psi} + u + f \tag{3.18}$$

A discretization of (3.18) yields

$$\dot{\psi}[k+1] = \Phi_{obs}\dot{\psi}[k] + \Gamma_{obs}(u[k] + f[k]) \tag{3.19}$$

where

$$\Phi_{obs} = e^{A_{obs}T_s} \tag{3.20}$$

$$\Gamma_{obs} = \frac{\Phi_{obs} - 1}{A_{obs}} \tag{3.21}$$

An observer which does not take the disturbance into account is given by

$$\dot{\hat{\psi}}[k+1] = \Phi_{obs}\dot{\hat{\psi}}[k] + \Gamma_{obs}u[k] + K(\dot{\psi}[k]) - \dot{\hat{\psi}}[k]) \tag{3.22}$$

Choosing $K = \Phi_{obs} - z_1$ will place the observer pole in an arbitrary position z_1. The estimation error is then

$$\dot{\tilde{\psi}}[k+1] = z_1\dot{\tilde{\psi}}[k] + \Gamma_{obs}f[k] \tag{3.23}$$

An estimate of the disturbance is now obtained by solving (3.23) for $f[k]$.

$$\hat{f}[k] = \frac{1}{\Gamma_{obs}}\left(\dot{\tilde{\psi}}[k+1] - z_1\dot{\tilde{\psi}}[k]\right) \tag{3.24}$$

A delay is introduced as in Section 3.2 and an estimate of the side wind $S_w[k]$ is obtained via (3.17).

$$\widehat{S}_w[k] = \frac{J}{e+\frac{\rho}{\sigma}}\hat{f}[k] = \frac{J}{\Gamma_{obs}\left(e+\frac{\rho}{\sigma}\right)}\left(\dot{\tilde{\psi}}[k] - z_1\dot{\tilde{\psi}}[k-1]\right) \tag{3.25}$$

Since the disturbance observer is first-order, it can not distinguish between a side wind disturbance and other disturbances, e.g. offset in a sensor. In Section 3.4.4 it is shown how the same structure may be used to estimate offset in the a_y-sensor. It is fully possible to design a second-order observer which is able to distinguish between two different disturbances, e.g. S_w and Φ_R, but it increases the complexity.

3.4 Robustness of the Side Wind Estimation

The robustness towards sensor offset and parameter error will be investigated in the following sections. Both effects give rise to falsely estimated side wind.

3.4.1 Sensitivity to Sensor Offset

To evaluate the effect of sensor offset, equation (3.18) will be used. In stationary, it becomes

$$0 = A_{obs}\dot{\psi} + u + f \tag{3.26}$$

By introducing offsets $\Delta\dot{\psi}$, $\Delta\delta$ and Δa_y it is possible to calculate to which side wind ΔS_w they correspond. Inserting the offsets according to (3.16)-(3.17), the following is obtained.

$$\Delta S_w = \frac{1}{e+\frac{\rho}{\sigma}}\left(\frac{L^2C_fC_r}{\sigma v_x}\Delta\dot{\psi} - \frac{LC_fC_r}{\sigma}\Delta\delta - \frac{m\rho}{\sigma}\Delta a_y\right) \tag{3.27}$$

Clearly, the sensitivity to offsets in lateral acceleration and steering angle is independent of v_x while the sensitivity to offsets in $\dot{\psi}$ increases for smaller values of v_x. For a Mercedes A-class, driving at 120 km/h, an offset of 1 $^\circ/s$ in the yaw rate sensor corresponds to a side wind of approximately 246 N while the same offsets corresponds to approximately 493 N when driving at 60 km/h. An offset of one degree in the sensored steering wheel angle, δ_{LR}, corresponds to approximately 180-190 N.

One way of reducing the effects of sensor offset is to introduce a lower limit on the estimated side wind which needs to be reached before any control action is taken. By switching the estimation off when v_x is below a certain limit, the sensitivity to offset in the $\dot{\psi}$-sensor is lowered. By passing the estimated side wind through a high-pass filter it is possible to reduce the effects without loosing the ability to suppress dynamic disturbances. There is also ongoing work which aims at estimating and removing the offsets themselves.

The sensor in the EPS-system which measures the steering wheel angle has a resolution of 1.5 degrees. It may therefore be favorable to avoid using this signal when estimating side wind. The measurements of the moment on the steering rod, M_{LR}, and of the angular speed of the steering wheel, $\dot{\delta}_{LR}$, are more reliable. In the following sections a few attempts at using this information in order to improve on the estimation of side wind are presented.

3.4.2 A Moment-Based Estimate

The idea of a moment-based estimate is to derive an estimate of the side wind using the measured moment on the steering rod instead of the measured steering wheel angle. Consider Figure 2.7 where the forces and moments acting on the steering system are shown. Under the assumptions $\ddot{\delta} = \dot{\delta} = 0$ and $i_L\delta = \delta_{LR}$, (2.44) becomes $i_L M_{LR} = n_k S_f$. Solving for S_f yields

$$S_f = \frac{i_L}{n_k} M_{LR} \tag{3.28}$$

It is then possible to rewrite (2.29) in the following manner.

$$J\ddot{\psi} = \frac{l_f i_L}{n_k} M_{LR} - l_r S_r + e S_w \tag{3.29}$$

The expression for S_r, as given in (2.20), is repeated here for convenience.

$$S_r = Cr\left(-\frac{v_y}{v_x} + \frac{l_r}{v_x}\dot{\psi}\right) \tag{3.30}$$

Since v_y is not measured, (3.30) needs to be rewritten in some way. In Section 3.3 this was solved by expressing $\frac{v_y}{v_x}$ in $\dot{\psi}$, a_y, S_w and δ, see (3.13). In order to rewrite it further, an expression for δ is needed.

By putting (3.28) equal to (2.19) and solving for $C_f\delta$ the following is obtained

$$C_f\delta = \frac{i_L}{n_k}M_{LR} + C_f\frac{v_y}{v_x} + \frac{l_f C_f}{v_x}\dot{\psi} \tag{3.31}$$

Inserting this expression in (3.13) yields the following equation

$$\frac{v_y}{v_x} = \frac{1}{\sigma}\left(\left(\frac{\rho}{v_x} + \frac{l_f C_f}{v_x}\right)\dot{\psi} + \frac{i_L}{n_k}M_{LR} + C_f\frac{v_y}{v_x} + S_w - ma_y\right) \tag{3.32}$$

By solving this for $\frac{v_y}{v_x}$ an expression which does not contain δ or v_y is obtained. Inserted in (3.30) it produces

$$S_r = ma_y - \frac{i_L}{n_k}M_{LR} - Sw \tag{3.33}$$

which may be inserted in (3.29), resulting in

$$J\ddot{\psi} = \frac{Li_L}{n_k}M_{LR} + (l_r + e)S_w - l_r ma_y \tag{3.34}$$

An estimate of S_w is then given by

$$\widehat{S}_w = \frac{1}{l_r + e}\left(J\ddot{\psi} - \frac{Li_L}{n_k}M_{LR} + l_r ma_y\right) \tag{3.35}$$

This estimate of S_w does not rely on the measured steering wheel angle. There are, however, drawbacks to this approach. CASCaDE was used to simulate a Mercedes S-class driving past side wind. As can be seen in Figure 3.1 the steady-state estimate does not coincide with that of the first-order observer. There are several possible explanations for this. For instance, there may be additional frictions and torques which have not been included in the model. Also, since the second-order system which connects the moment and the steering angle has been disregarded, the estimate will be very sensitive towards transients in the maneuvers.

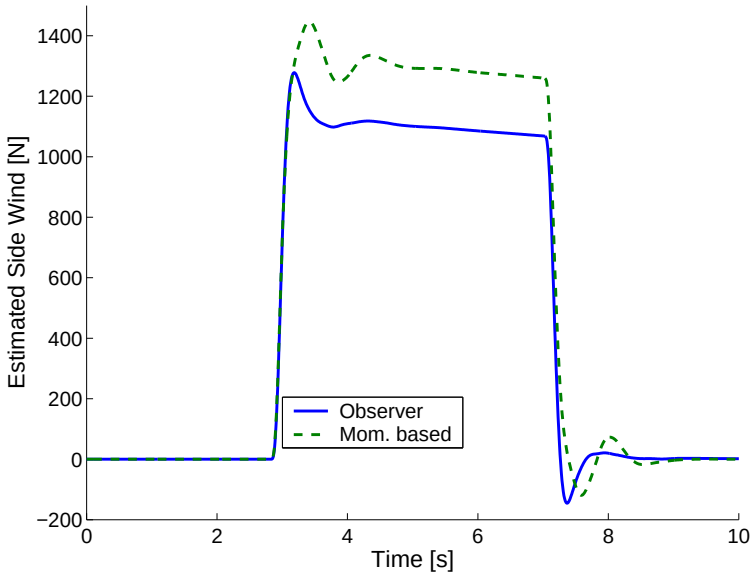

Figure 3.1: Estimated side wind using the first-order observer and the moment-based estimate.

3.4.3 Smoothing δ_{LR}

The quantization of the measured steering wheel angle does not originate from round-off but from how the sensor is constructed. When the signal from the sensor changes, it outputs the correct angle of the steering wheel at that instant of time. However, between the changes it does not provide any information about the angle except that it is in a region of ± 1.5 degrees of the current value. One way of improving on this is to use other sensored signals to estimate δ_{LR} in these intervals. This will be done by designing a switched system which makes use of the measured angular velocity of the steering wheel.

The definition of a change at time k is given in (3.36). When this is fulfilled $\delta_{LR}^m[k]$ is considered to be accurate[1].

$$\delta_{LR}^m[k] - \delta_{LR}^m[k-1] \neq 0 \tag{3.36}$$

Instead of setting $\hat{\delta}_{LR}[k] = \delta_{LR}^m[k]$ at the instants where the measurement is accurate $\hat{\delta}_{LR}$ will approach this value as a dynamical system. Setting a fixed value for the estimated angle would counteract the goal of obtaining a smoother signal. Therefore, the following dynamics for $\hat{\delta}_{LR}$ is used when (3.36) is fulfilled.

[1]The superscript ^{m} will be used to denote measured signals throughout this section in order to distinguish them from the estimated, and real, ones.

$$\hat{\delta}_{LR}[k+1] = (1 - KT_s)\hat{\delta}_{LR}[k] + KT_s\delta_{LR}^m[k] \tag{3.37}$$

The system pole is placed in $1 - KT_s$ which makes it asymptotically stable as long as $K \in (0, \frac{2}{T_s})$. If the system was to remain in this state, and K was chosen in the specified interval, the estimate would converge to the measured value. The rate of convergence is determined by the value of K. A large K will provide a good fit to the measured values but also a rather messy signal. A small value will conversely produce a smooth signal but less fitting.

During these intervals the fact that the derivative of the estimated steering wheel angle should be equal to the measured angular velocity of the steering wheel will be used. By the approximation $\dot{\hat{\delta}}_{LR}[k] \approx \frac{1}{T_s}\left(\hat{\delta}_{LR}[k] - \hat{\delta}_{LR}[k-1]\right)$ the following dynamics for this state are obtained.

$$\hat{\delta}_{LR}[k+1] = \hat{\delta}_{LR}[k] + T_s\dot{\delta}_{LR}^m[k] \tag{3.38}$$

To sum things up, the system may be presented in the following manner.

$$\hat{\delta}_{LR}[k+1] = \begin{cases} (1 - KT_s)\hat{\delta}_{LR}[k] + KT_s\delta_{LR}^m[k] & \text{when (3.36) is fulfilled} \\ \hat{\delta}_{LR}[k] + T_s\dot{\delta}_{LR}^m[k] & \text{otherwise} \end{cases} \tag{3.39}$$

Finally, a pragmatic solution to the choice of K is applied. By choosing K large and passing the estimated signal through a low-pass filter good fitting to the measured values is achieved while keeping the signal relatively smooth. In Figure 3.2 the sensored signal and the estimate are plotted. The use of the measured angular velocity evidently provides reasonable transitions between the measured points. Initially, the estimate is incorrect, since no changes occur and the angular velocity is zero.

3.4.4 Estimation of Sensor Offset

The first-order disturbance observer, which was derived in Chapter 3.3, only requires small variations to yield an estimate of the offset in the a_y-sensor. It is assumed that the sensored lateral acceleration, a_y^{sens} is the sum of the actual acceleration and an offset.

$$a_y^{sens} = a_y + a_y^o \tag{3.40}$$

Solving for a_y and inserting the expression into (3.14) yields an equation for yaw rate which has side wind and a_y^o as disturbances. Since only one of these

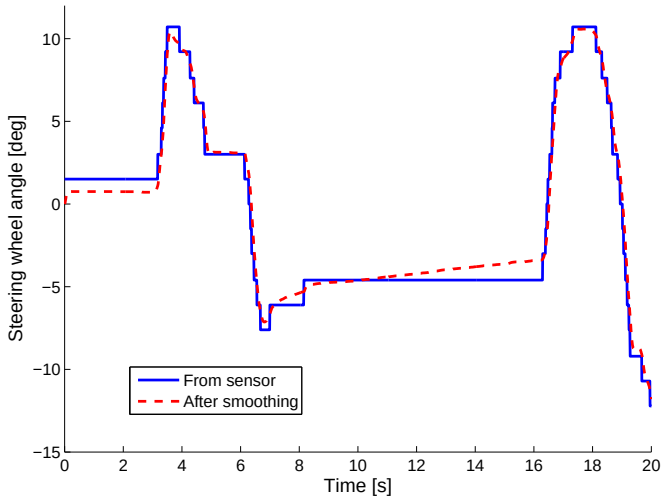

Figure 3.2: Steering wheel angle from sensor before and after smoothing.

may be identified by the first-order observer, the term containing side wind is discarded, which leaves the following equation.

$$\ddot{\psi} = -\frac{L^2 C_f C_r}{J\sigma v_x}\dot{\psi} - \frac{m\rho}{J\sigma}\left(a_y^s - a_y^o\right) + \frac{LC_f C_r}{J\sigma}\delta \tag{3.41}$$

By introducing the following notations,

$$A_{obs} = -\frac{L^2 C_f C_r}{J\sigma v_x}, \quad u = -\frac{m\rho}{J\sigma}a_y^s + \frac{LC_f C_r}{J\sigma}\delta, \quad f = \frac{m\rho}{J\sigma}a_y^o \tag{3.42}$$

the system has the same form as (3.18), which is repeated here.

$$\ddot{\psi} = A_{obs}\dot{\psi} + u + f \tag{3.43}$$

After discretization, an estimate of f is obtained in the same way as in Section 3.3, resulting in

$$\hat{f}[k] \approx \hat{f}[k-1] \approx \frac{1}{\Gamma_{obs}}\left(\dot{\hat{\psi}}[k] - z_1\dot{\hat{\psi}}[k-1]\right) \tag{3.44}$$

The difference this time lies only in that the disturbance is interpreted as sensor offset instead of side wind. An estimate of the offset is given by the following expression.

$$a_y^o[k] = \frac{J\sigma}{m\rho}\hat{f}[k] \approx \frac{J\sigma}{m\rho\Gamma_{obs}}\left(\dot{\hat{\psi}}[k] - z_1\dot{\hat{\psi}}[k-1]\right) \tag{3.45}$$

3.4.5 Sensitivity to Parameter Error

When the parameters of the side wind observer are incorrect, each turn will generate an error in the observer which is interpreted as side wind. To determine how large this effect is, the continuous time transfer function between δ and $\widehat{S}_w$ will be calculated. The obtained transfer function is not realizable, which makes it interesting to compare the results to those obtained from simulation in Simulink.

The continuous time one-track model from Section 2.4 will be used as 'real' vehicle and be combined with a continuous-time version of the first order observer according to Figure 3.3.

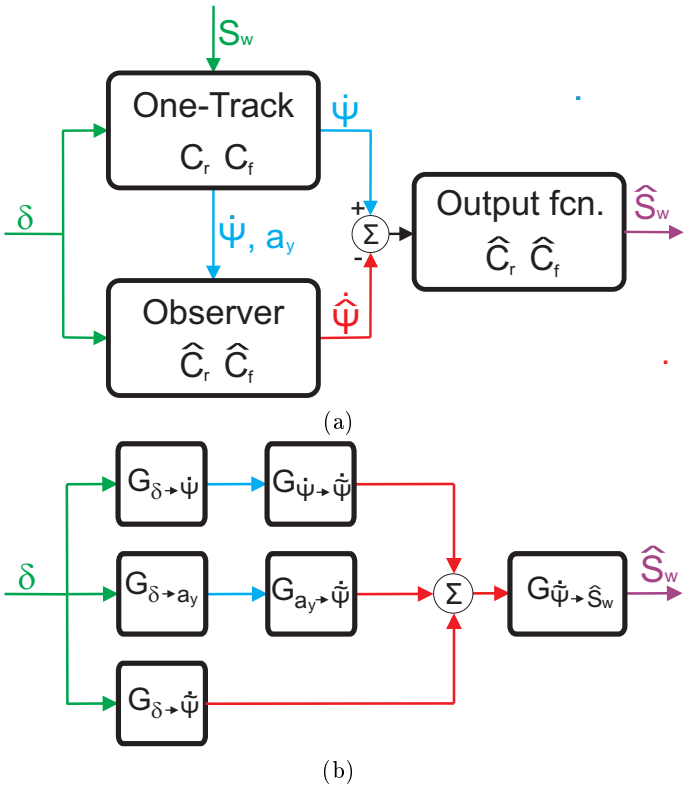

Figure 3.3: (a) A sketch of how the sensitivity to model error is investigated and (b) the corresponding block diagram with the relevant transfer functions.

The transfer functions from δ to $\dot{\psi}$ and a_y are calculated using the matrices in (2.32) and the equality $G(s) = C(sI - A)^{-1}B + D$. The matrices G and

H are disregarded since δ is the interesting input for this investigation.

$$G_{\delta\to\dot{\psi}} = \frac{(l_f C_f s + LC_f C_r/mv_x)/J}{s^2 + (J\sigma + m\kappa)\, s/Jmv_x + (L^2 C_f C_r + \rho m v_x^2)/Jmv_x^2} \tag{3.46}$$

$$G_{\delta\to a_y} = \frac{(C_f/m)s^2 + (Ll_r C_f C_r/Jmv_x)s + LC_f C_r/Jm}{s^2 + (J\sigma + m\kappa)\, s/Jmv_x + (L^2 C_f C_r + \rho m v_x^2)/Jmv_x^2} \tag{3.47}$$

The continuous disturbance observer will be based on Equation (3.14), which yields the following observer equation.

$$\ddot{\hat{\psi}} = -\frac{L^2 C_f C_r}{J\sigma v_x}\dot{\hat{\psi}} - \frac{m\rho}{J\sigma}a_y + \frac{LC_f C_r}{J\sigma}\delta + K(\dot{\psi} - \dot{\hat{\psi}}) \tag{3.48}$$

The definition of A_{obs} is repeated here, and two new notations are introduced.

$$A_{obs} = -\frac{L^2 C_f C_r}{J\sigma v_x} \tag{3.49}$$

$$B_{1,obs} = -\frac{m\rho}{J\sigma} \tag{3.50}$$

$$B_{2,obs} = \frac{LC_f C_r}{J\sigma} \tag{3.51}$$

With $K = A_{obs} - z_1$, the following equality holds.

$$\dot{\hat{\psi}} = \frac{B_{1,obs}a_y + B_{2,obs}\delta + (A_{obs} - z_1)\dot{\psi}}{s - z_1} \tag{3.52}$$

The transfer function from δ, a_y and $\dot{\psi}$ to the observer error $\dot{\tilde{\psi}}$ is then

$$G_{\delta\to\dot{\tilde{\psi}}} = -\frac{B_{2,obs}}{s - z_1} \tag{3.53}$$

$$G_{a_y\to\dot{\tilde{\psi}}} = -\frac{B_{1,obs}}{s - z_1} \tag{3.54}$$

$$G_{\dot{\psi}\to\dot{\tilde{\psi}}} = \frac{s - A_{obs}}{s - z_1} \tag{3.55}$$

The transfer function from $\dot{\tilde{\psi}}$ to $\widehat{S}_w$ is now needed. The observer error is given by

$$\ddot{\tilde{\psi}} = (A_{obs} - K)\dot{\tilde{\psi}} + f = z_1\dot{\tilde{\psi}} + f \tag{3.56}$$

An estimate of S_w is then obtained via (3.17) and solving (3.56) for f.

$$\widehat{S}_w = \frac{J}{e + \rho/\sigma}\hat{f} = \frac{J}{e + \rho/\sigma}(s - z_1)\dot{\tilde{\psi}} \tag{3.57}$$

which provides the last required transfer function

$$G_{\dot{\tilde{\psi}} \to \widehat{S}_w} = \frac{J}{e + \rho/\sigma}(s - z_1) \tag{3.58}$$

The transfer function from δ to S_w is given by

$$G_{\delta \to \widehat{S}_w} = \left(G_{\delta \to \dot{\tilde{\psi}}} + G_{\delta \to a_y} G_{a_y \to \dot{\tilde{\psi}}} + G_{\delta \to \dot{\psi}} \quad G_{\dot{\psi} \to \dot{\tilde{\psi}}} \right) G_{\dot{\tilde{\psi}} \to \widehat{S}_w} \tag{3.59}$$

Parameter error may then be modeled by replacing C_f and C_r with $\widehat{C}_f$ and $\widehat{C}_r$ in the transfer functions connected to the observer while leaving (3.46) and (3.47) unaltered. Note that the observer pole in $s = z_1$ will be canceled regardless of parameter error. When the parameters in the observer are correct, the transfer function from S_w to $\widehat{S}_w$ is one and the one from δ to $\widehat{S}_w$ is zero. However, when the parameters are incorrect, each degree steering angle will generate a certain estimated side wind. To investigate this, Matlab was used to draw bode diagrams. In order to make the results easier to relate to, the amplitude diagram is scaled so that it represents the transfer function from steering wheel angle δ_{LR} instead of δ.

In Figure 3.4 the bode diagrams are displayed when varying each of the parameters independently. The parameters where chosen according to $\widehat{C}_f = k \cdot C_f$ and $\widehat{C}_r = k \cdot C_r$ where $k \in \{0.7\ 0.95\ 1\ 1.05\ 1.3\}$. The phase diagram indicates that the sign is reversed when $\widehat{C}_f$ is increased or $\widehat{C}_r$ is decreased. It also seems that the most sensitive parameter is $\widehat{C}_f$, which produces almost 80 N of estimated side wind per degree steering wheel angle when it is chosen 30% higher than C_f.

To investigate the effects of discretization, the continuous-time vehicle model was implemented in Simulink. The outputs $\dot{\psi}$ and a_y were sampled using zero order hold and used as inputs to the discrete-time observer derived in Section 3.3. The velocity was kept constant and the steering input consisted of sinusoids with varying frequency. Figure 3.5 displays the gain diagram from steering wheel angle to estimated side wind for three choices of sample time when there was no parameter error in the observer.

Apparently, a larger value of T_s generates more falsely estimated side wind. The error is also increasing with the frequency. These effects are intuitively explained by the fact that the estimation error is equal to the change in disturbance over the last two samples. Increasing the frequency for a given sample time then has the same effect as increasing the sample time for a given frequency.

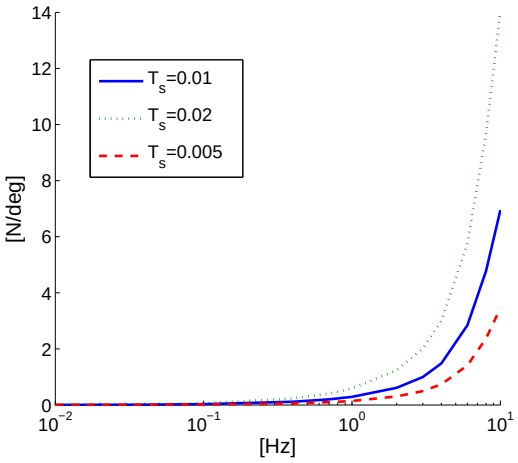

Figure 3.5: Amplitude diagram between δ_{LR} and $\widehat{S}_w$ with T_s=0.01, 0.02 and 0.005.

Figure 3.6 displays the amplitude diagrams from δ_{LR} to $\widehat{S}_w$ when C_f and C_r are varied and the sample time was set to 0.01. The results are fairly similar to those of the analytical calculations. Clearly, incorrect parameters in the observer affects the performance rather heavily. In order to avoid this, on line estimation of a few parameters will be attempted in the following chapter.

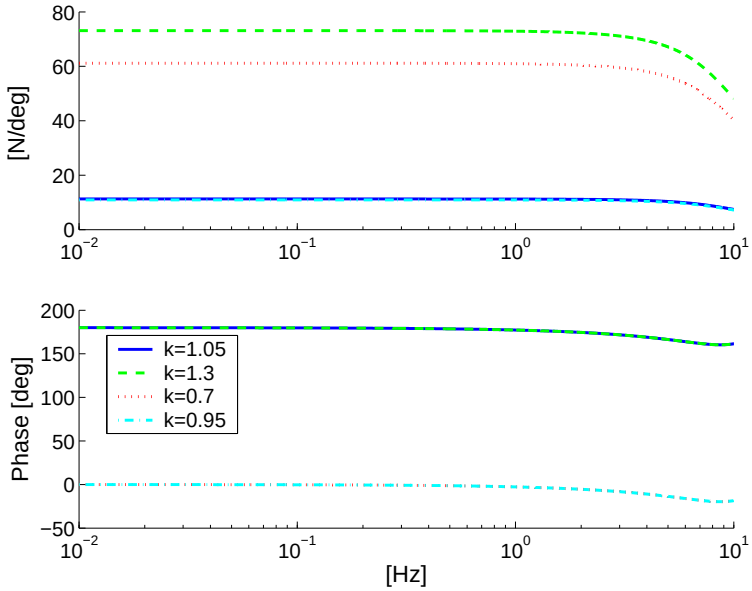

(a) Variations in $\widehat{C}_f$.

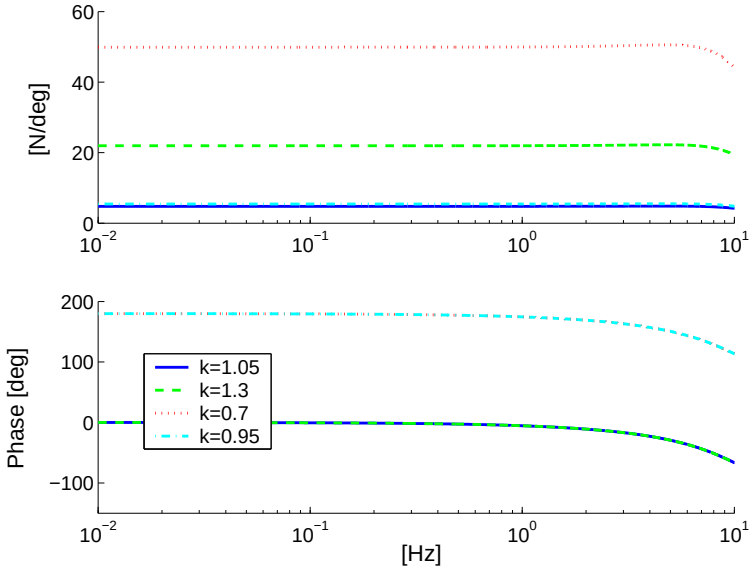

(b) Variations in $\widehat{C}_r$.

Figure 3.4: Bode diagram of the continuous-time transfer function from δ_{LR} to $\widehat{S}_w$ with $\widehat{C}_f = k \cdot C_f$ and $\widehat{C}_r = k \cdot C_r$ for k = 1.05, 1.3, 0.7, and 0.95. The magnitude is given in N estimated side wind per degree steering wheel angle.

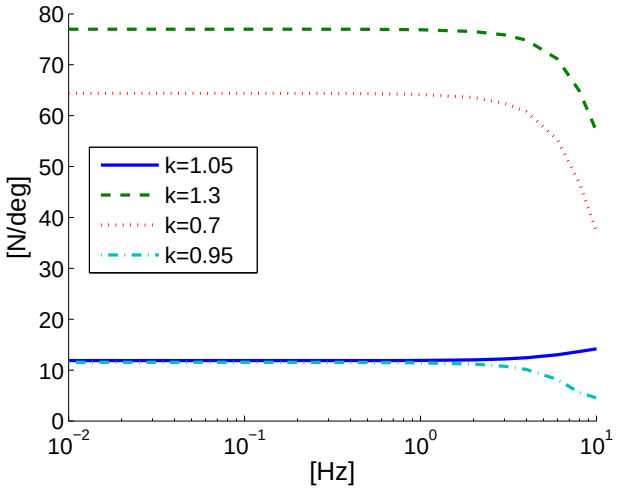

(a) Variations in $\widehat{C}_f$.

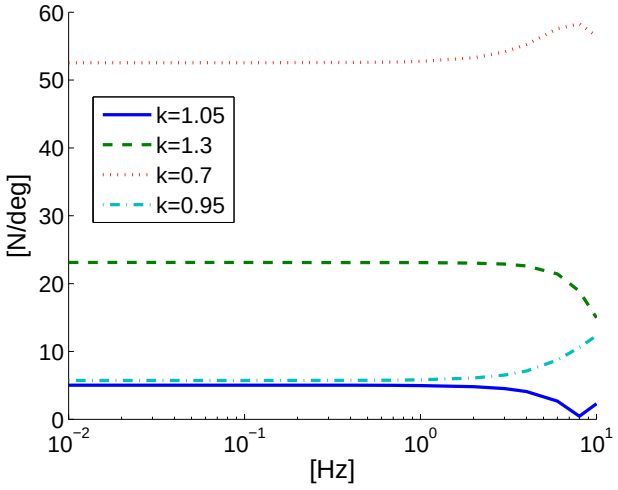

(b) Variations in $\widehat{C}_r$.

Figure 3.6: Amplitude diagram between δ_{LR} and $\widehat{S}_w$ from simulation with $\widehat{C}_f = k \cdot C_f$ and $\widehat{C}_r = k \cdot C_r$ for k = 1.05, 1.3, 0.7, and 0.95. The magnitude is given in N estimated side wind per degree steering wheel angle.

Chapter 4

On Line Parameter Estimation

As was shown in Section 3.4.5, the effects of inaccurate parameters in the one-track vehicle model are quite large and it is therefore necessary to make the model adaptive in order to improve performance. Some parameters, such as the length of the vehicle, will not be subject to change while others, such as the mass and the position of the center of gravity, will fluctuate between different driving sessions. One possible implementation is to perform identification of a few critical parameters at low speed and then use the estimated values at higher speeds, when the side wind compensation is actually needed, see Figure 4.1.

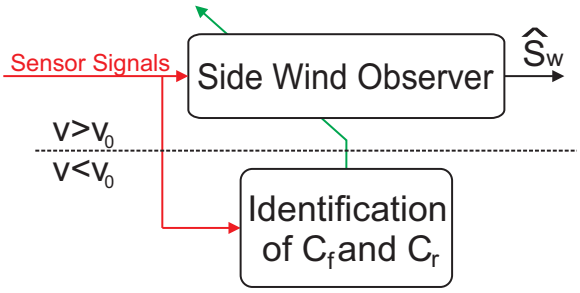

Figure 4.1: A possible way of switching between parameter identification and side wind estimation.

The following sections present attempts at identifying the cornering stiffness of the front and rear tyre. Choosing these parameters for identification is reasonable since they are very likely to change between different driving sessions depending on the weather and the choice of tyres. Note that the identification is performed under the assumption that there are no disturbances acting on the vehicle. A previous investigation of on line identification in vehicles is presented in [14].

4.1 Least Squares Estimation

The main idea of least squares estimation is to fit input data and output data in a linear fashion. The following introduction is based on [8] and [9]. Assume that a system is governed by the following equation.

$$y[t] = \boldsymbol{\phi}^T[t]\boldsymbol{\theta} = \phi_1[t]\theta_1 + \phi_2[t]\theta_2 + \ldots + \phi_N[t]\theta_N \tag{4.1}$$

The vector $\boldsymbol{\theta}$ contains the parameters which are to be identified, ϕ_i are known functions and y is some known output. The least squares estimate of $\boldsymbol{\theta}$, denoted $\hat{\boldsymbol{\theta}}$, is then chosen such that it minimizes the cost function

$$Q(\boldsymbol{\theta}, t) = \frac{1}{2}\sum_{k=1}^{t}(y[k] - \boldsymbol{\phi}^T[k]\boldsymbol{\theta})^2 \tag{4.2}$$

This means that the error will be penalized quadratically. It can be proved that the cost function is minimized by estimates $\hat{\boldsymbol{\theta}}$ which fulfill

$$\Phi^T\Phi\hat{\boldsymbol{\theta}} = \Phi^T Y \tag{4.3}$$

where

$$\Phi = \begin{pmatrix}\boldsymbol{\phi}^T[1] & \boldsymbol{\phi}^T[2] & \ldots & \boldsymbol{\phi}^T[t]\end{pmatrix}^T \tag{4.4}$$

$$Y = \begin{pmatrix}y[1] & y[2] & \ldots & y[t]\end{pmatrix}^T \tag{4.5}$$

Equation (4.3) is known as the *normal equation* and when the inverse of $\Phi^T\Phi$ exists it has the unique solution

$$\hat{\boldsymbol{\theta}} = \left(\Phi^T\Phi\right)^{-1}\Phi^T Y \tag{4.6}$$

The requirement that the inverse of $\Phi^T\Phi$ exists may prove hard to fulfill under certain circumstances. It is connected with the notion of persistent excitation.

4.1.1 Persistent Excitation

Persistent excitation is a measure of how many parameters that may be estimated using, for instance, least squares estimation. If the input to the least squares estimation is persistently exciting of order n, n parameters may

be identified uniquely. In [9], persistent excitation is defined in the following way.

Definition 1. *A signal u fulfils the condition of persistent excitation (PE) of order n if the following limits exist.*

$$\bar{u} = lim_{N\to\infty}\frac{1}{N}\sum_{k=1}^{N} u_k \tag{4.7}$$

$$\widehat{C}_{uu}(\tau) = lim_{N\to\infty}\frac{1}{N}\sum_{k=1}^{N} u_k u_{k-\tau}^T \tag{4.8}$$

and if the correlation matrix

$$R_{uu}(n) = \begin{pmatrix} \widehat{C}_{uu}(0) & \widehat{C}_{uu}(1) & \dots & \widehat{C}_{uu}(n-1) \\ \widehat{C}_{uu}(-1) & \widehat{C}_{uu}(0) & \dots & \widehat{C}_{uu}(n-2) \\ \vdots & \vdots & \ddots & \vdots \\ \widehat{C}_{uu}(1-n) & \widehat{C}_{uu}(2-n) & \vdots & \widehat{C}_{uu}(0) \end{pmatrix} \tag{4.9}$$

is positive definite.

Since this is difficult to verify on line, a method involving singular values will be used. It suggests a singular value decomposition of $\Phi^T\Phi$. The number of uniquely identifiable parameters is then equal to the number of non-zero singular values. An indication as to why this holds will now be presented.

Singular Values and Least Squares Estimation

For further reading on the singular value decomposition, see [12]. Assume that $\Phi^T\Phi \in \mathbb{R}^{n\times n}$ and that it has the following singular value decomposition

$$\Phi^T\Phi = USV^T \tag{4.10}$$

where $U, V \in \mathbb{R}^{n\times n}$ are orthonormal and $S \in \mathbb{R}^{n\times n}$ is a matrix with the singular values of $\Phi^T\Phi$ along its diagonal and all other elements zero. This means that $U^T = U^{-1}$, $V^T = V^{-1}$ and that $S^T = S$. Equation (4.6) may then be rewritten as follows.

$$\hat{\theta} = \left(\Phi^T\Phi\right)^{-1}\Phi^T Y = \left(USV^T\right)^{-1}\Phi^T Y = VS^{-1}U^T\Phi^T Y \tag{4.11}$$

It is clear that the estimate will diverge if any of the diagonal elements of S are zero, since the determinant of S is

$$det(S) = \sigma_1\sigma_2\sigma_3 \dots \sigma_n \tag{4.12}$$

where σ_i denote the singular values of $\Phi^T\Phi$. However, it also indicates that problems may arise when any of the singular values of $\Phi^T\Phi$ are close to zero. One of the few ways of dealing with this is to avoid using singular values which are (almost) zero. This, in turn, means that fewer parameters may be identified.

4.1.2 The Recursive Algorithm

When used on line, least squares is usually applied via a recursive algorithm. One of the main advantages is that relatively few data points need to be stored, and it also facilitates estimation of time varying parameters. The following equations constitute a recursive least squares algorithm.

$$\hat{\boldsymbol{\theta}}[k] = \hat{\boldsymbol{\theta}}[k-1] + P[k]\boldsymbol{\phi}[k]\epsilon[k] \tag{4.13}$$

$$\epsilon[k] = y[k] - \boldsymbol{\phi}^T[k]\hat{\boldsymbol{\theta}}[k-1] \tag{4.14}$$

$$P[k] = \frac{1}{\lambda}\left(P[k-1] - \frac{P[k-1]\boldsymbol{\phi}[k]\boldsymbol{\phi}^T[k]P[k-1]}{\lambda + \boldsymbol{\phi}^T[k]P[k-1]\boldsymbol{\phi}[k]}\right) \tag{4.15}$$

The error between calculated and measured output at time k is denoted $\epsilon[k]$ and $P[k]$ is the covariance matrix at this instant. This version of recursive least squares includes a forgetting factor, $0 < \lambda \leq 1$, which attenuates the impact of older measurement data. This is especially useful when attempting to estimate time-varying parameters. The disadvantage of using a small value of λ is that the estimation becomes more sensitive to noise and other disturbances since the averaging effect is reduced. Another possible effect of setting λ to low is estimator windup, which is discussed in [8]. The problem occurs when there is insufficient excitation in the system and $\lambda < 1$. The covariance matrix P will then grow more or less exponentially, depending on how severe the shortage of excitation is. This makes the estimation perform rather poorly and also produces large transients in the estimate when the input is persistently exciting again. One way of avoiding this is to use conditional updating. This means that the least squares algorithm is modified so that the estimate and covariance matrix only are updated when there is enough excitation. Otherwise, the previous values are held. It is vital to choose a suitable criterion for when to allow updates as a trade-off

between risking estimator windup and using too few of the samples in the identification. A typical choice of criterion is one that ascertains that the magnitude of $\boldsymbol{\phi}^T[k]P[k-1]\boldsymbol{\phi}[k]$ is large enough.

When using recursive least squares, initial values for $\hat{\boldsymbol{\theta}}$ and P must be specified. With a bit of knowledge about the system it is possible to choose $\hat{\boldsymbol{\theta}}[0]$ in a region around it's actual value. When this is not the case, an alternative is to perform regular least squares over an initial set of data and use this estimate as initial value for the recursive algorithm. This technique also provides an initial value for P. Otherwise, it is fairly common to choose $P[0] = k_{P_0}I$ where k_{P_0} is a positive constant. A large value of k_{P_0} makes the first few steps larger, which may be convenient when the initial estimate of θ is a rough guess, but may also lead to large initial variations in the estimate.

4.1.3 LS1: Estimation of One Parameter

A least squares estimator which attempts to identify only one parameter will now be presented. The identification will be based on equation (3.18). Since it is assumed that no side wind is acting on the vehicle during the identification, the last term is excluded. This yields the following, continuous time, equation for yaw rate.

$$\ddot{\psi} = -\frac{L^2 C_f C_r}{J\sigma v_x}\dot{\psi} - \frac{m\rho}{J\sigma}a_y + \frac{LC_fC_r}{J\sigma}\delta \tag{4.16}$$

By choosing

$$y_1 = C_r J\ddot{\psi} + l_r C_r m a_y \quad \theta_1 = C_f \quad \phi_1 = -\tfrac{C_r L^2}{v_x}\dot{\psi} + l_f m a_y + C_r L\delta \tag{4.17}$$

equation (4.16) may be written $y_1 = \phi_1^T\theta_1$. Since $\ddot{\psi}$ can not be measured, the Euler approximation $\ddot{\psi}[t] \approx \left(\dot{\psi}[t] - \dot{\psi}[t-1]\right)/T_s$ may be used.

4.1.4 LS2: Estimation of Two Parameters

Identifying both C_r and C_f is not entirely straight forward. This is due to the fact that they enter the equations of the one track model in a non-linear fashion. Since linearity in parameters is a necessity for least squares estimation, an indirect approach will be attempted. By choosing

$$y_2 = \ddot{\psi} \quad \boldsymbol{\theta}_2^T = \begin{pmatrix} \frac{C_fC_r}{\sigma} & \frac{\rho}{\sigma} \end{pmatrix} \quad \boldsymbol{\phi}_2^T = \begin{pmatrix} -\frac{L^2}{Jv_x}\dot{\psi} + \frac{L}{J}\delta & -\frac{m}{J}a_y \end{pmatrix} \tag{4.18}$$

equation (4.16) may be written $y_2 = \boldsymbol{\phi}_2^T \boldsymbol{\theta}_2$. The parameters $\widehat{C}_f$ and $\widehat{C}_r$ may then be calculated from $\hat{\theta}_2$ at each step according to

$$\widehat{C}_r[k] = \frac{\hat{\theta}_{2,1}[k]L}{l_r - \hat{\theta}_{2,2}[k]}, \quad \widehat{C}_f[k] = \frac{\hat{\theta}_{2,1}[k]L}{l_f + \hat{\theta}_{2,2}[k]} \tag{4.19}$$

where $\hat{\theta}_{2,1}$ and $\hat{\theta}_{2,2}$ denote the first and second element of $\hat{\boldsymbol{\theta}}_2$.

To make use of the strategy proposed in Chapter 4.1.1 the regressor matrix Φ_N is formed according to

$$\Phi_N = \begin{pmatrix} \phi_{2,1}[1] & \phi_{2,2}[1] \\ \phi_{2,1}[2] & \phi_{2,2}[2] \\ \vdots & \vdots \\ \phi_{2,1}[N] & \phi_{2,2}[N] \end{pmatrix} \tag{4.20}$$

where $\phi_{2,1}$ and $\phi_{2,2}$ denote the first and second row of ϕ_2. The product $\Phi_N^T \Phi_N$ is then

$$\Phi_N^T \Phi_N = \begin{pmatrix} \sum_{k=1}^N \phi_{2,1}^2[k] & \sum_{k=1}^N \phi_{2,1}[k]\phi_{2,2}[k] \\ \sum_{k=1}^N \phi_{2,1}[k]\phi_{2,2}[k] & \sum_{k=1}^N \phi_{2,2}^2[k] \end{pmatrix} \tag{4.21}$$

One might hold an objection against the singular value-criterion when a forgetting factor is used. When $\lambda < 1$, older input values will have less impact on the result. The singular value decomposition, however, will take all past input values into account. This means that if the first j samples are persistently exciting of order n and $\phi[k] = 0$ for $k > j$, the singular value test would still consider the input persistently exciting of order n for all future samples. Two suggestions on how to compensate for this will be presented in the following section.

4.1.5 Introducing a Forgetting Factor in the SVD-test

Since older input values to the RLS-estimation will be weighted with λ, it seems reasonable to do the same when evaluating the number of identifiable parameters. One way of doing this is to introduce $\Phi_N(\lambda)$ according to the following

$$\Phi_N(\lambda) = \begin{pmatrix} \lambda^{N-1}\phi_{2,1}[1] & \lambda^{N-1}\phi_{2,2}[1] \\ \lambda^{N-2}\phi_{2,1}[2] & \lambda^{N-2}\phi_{2,2}[2] \\ \vdots & \vdots \\ \lambda^{0}\phi_{2,1}[N] & \lambda^{0}\phi_{2,2}[N] \end{pmatrix} \tag{4.22}$$

As $N \to \infty$ older data points tend to zero, and thus do not affect $\Phi_N^T(\lambda)\Phi_N(\lambda)$. When $\lambda = 1$, the results are the same as when using the original test. The modification yields the following product $\Phi_N^T(\lambda)\Phi_N(\lambda)$, for which the singular values can be calculated.

$$\Phi_N^T(\lambda)\Phi_N(\lambda) = \begin{pmatrix} \sum_{k=1}^{N}\left(\lambda^{N-k}\phi_{2,1}[k]\right)^2 & \sum_{k=1}^{N}\left(\lambda^{N-k}\right)^2\phi_{2,1}[k]\phi_{2,2}[k] \\ \sum_{k=1}^{N}\left(\lambda^{N-k}\right)^2\phi_{2,1}[k]\phi_{2,2}[k] & \sum_{k=1}^{N}\left(\lambda^{N-k}\phi_{2,2}[k]\right)^2 \end{pmatrix} \tag{4.23}$$

Another option is to use the following approximate expression for the number of samples which are used at each step, [9].

$$N_\lambda = \frac{1}{1-\lambda} \tag{4.24}$$

It is then possible to perform the singular value decomposition using only the last N_λ samples, which might give more realistic information regarding the input at a specific time. This modification is also consistent with the original test for $\lambda = 1$ since the number of samples tends to infinity as $\lambda \to 1$. Both suggestions will be applied to measurement data in Section 4.3.2, but need to be investigated further.

4.2 Multiple Model Estimation

The main idea in Multiple Model Estimation (MME) is to run several models in parallel and determine which of the models that produces the best fit to measured data according to some criterion. In this case it will be used to identify parameters in a parametric model, but it may also be used to choose between different model structures. One advantage with this method is that it chooses its estimate from a pre-defined library which makes it possible to avoid estimates that are unrealistic. It is also fast and does not require a model which is linear in the parameters. The following, brief, introduction is based on [5].

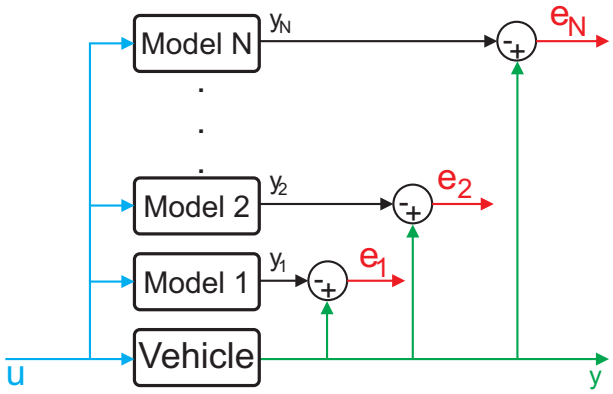

Figure 4.2: Sketch of how e_i are obtained using Multiple Model Estimation

Consider the following, linear, system where $\boldsymbol{\phi} \in \mathbb{R}^m$ is the input, $\boldsymbol{y} \in \mathbb{R}^p$ is the output and $\boldsymbol{\theta} \in \mathbb{R}^n$ contains the unknown parameters. Note that f may be nonlinear.

$$y[k] = f(\boldsymbol{\theta}, \boldsymbol{\phi}[k-1]), \quad f : \mathbb{R}^m \times \mathbb{R}^n \Rightarrow \mathbb{R}^p \tag{4.25}$$

Initially, N separate parameter sets $\boldsymbol{\theta}_1, \boldsymbol{\theta}_2, \ldots, \boldsymbol{\theta}_N$ are chosen to form a library from which the estimator makes its choice. With a bit of knowledge about the system they may be chosen from the set of feasible parameter values, denoted Θ. One model for each parameter set is created and the calculated outputs $\hat{\boldsymbol{y}}_i[k] = f(\boldsymbol{\theta}_i, \boldsymbol{\phi}[k-1])$ are compared to the measured output $\boldsymbol{y}[k]$ to obtain the errors $\boldsymbol{e}_i$. A sketch of this step is presented in Figure 4.2.

$$\boldsymbol{e}_i[k] = \boldsymbol{y}[k] - \hat{\boldsymbol{y}}_i[k], \quad i = 1 \ldots N \tag{4.26}$$

Some weight function $Q(\boldsymbol{e})$ may then be applied to the error signals and the parameter estimate is chosen according to

$$\hat{\boldsymbol{\theta}} = \boldsymbol{\theta}_j, \quad j = \left\{ 1 \leq j \leq N \;\middle|\; Q(\boldsymbol{e}_j) = \min_{i \in [1,N]} Q(\boldsymbol{e}_i) \right\} \tag{4.27}$$

This means that, even when the identification fails, the parameter estimate will produce a stable and realistic model of the system as long as $\boldsymbol{\theta}_i \in \Theta$ for all i. There are three design parameters in this approach to MME; the choice of parameter library, error function, and weight function.

Switching Hysteresis

If two estimates in the library, θ_p and θ_q, produce almost the same weighted error, so called *chattering* may occur. This means that the algorithm switches between the two infinitely. One way of avoiding, or at least reducing, this effect is to introduce a switching hysteresis.

The hysteresis is introduced according to [13] such that switching only takes place when $Q(e_q)(1+h) \leq Q(e_p)$ (or the other way around), where h is a design parameter. This ascertains that the new estimate is sufficiently better than the current.

Three attempts at multiple model estimation will now be presented, with $\boldsymbol{\theta} = (C_r \quad C_f)^T$.

4.2.1 MME 1: Error Equation

A first approach is to determine how accurately each parameter set fulfills (3.18) under the assumption that no side wind is acting on the car. The notations defined in (4.18) are used, so that equation (3.18) may be written on the following form.

$$y_2(t) = \boldsymbol{\phi}_2^T(t)\boldsymbol{\theta}_2$$

Each parameter set $\boldsymbol{\theta}_{2_i}$ then yields the following output

$$\hat{y}_{2_i}(t) = \boldsymbol{\phi}_2^T(t)\boldsymbol{\theta}_{2_i}$$

The corresponding errors $e_i(t) = y_2(t) - \hat{y}_{2_i}(t)$ are given by

$$e_i(t) = \boldsymbol{\phi}_2^T(t)\left(\boldsymbol{\theta}_2 - \boldsymbol{\theta}_{2_i}\right) \tag{4.28}$$

The weight function is chosen according to

$$Q(e_i(t)) = \int_0^t H(\tau)e_i^2(t-\tau)d\tau \tag{4.29}$$

where $H(\tau)$ is a first-order low pass filter on the following form.

$$H(s) = \frac{1}{s+T_f}$$

This choice of $Q(e)$ introduces a certain degree of integration depending on the choice of T_f. When $T_f = 0$, $H(s)$ is a pure integrator which corresponds to weighting all time steps equally. As T_f increases, older time steps will be less and less important. This weight function will be used in all three versions of MME presented in this thesis, the difference lies in how the error signals e_i are obtained.

Laplace transformation of Equation (4.29) yields

$$Q(e_i(s)) = H(s)e_i^2(s) \tag{4.30}$$

By inserting (4.28), the following is obtained

$$Q(e_i(s)) = H(s)\boldsymbol{\phi}_2^T(s)(\boldsymbol{\theta}_2 - \boldsymbol{\theta}_{2_i})$$

Multiplication with $\boldsymbol{\phi}_2(s)$ yields

$$\boldsymbol{\phi}_2(s)Q(e_i(s)) = H(s)\boldsymbol{\phi}_2(s)\boldsymbol{\phi}_2^T(s)(\boldsymbol{\theta}_2 - \boldsymbol{\theta}_{2_i})$$

The parameter error $\tilde{\boldsymbol{\theta}}_2 = \boldsymbol{\theta}_2 - \boldsymbol{\theta}_{2_i}$ is then given by

$$\tilde{\boldsymbol{\theta}}_2 = H^{-1}\left(\boldsymbol{\phi}_2(s)\boldsymbol{\phi}_2^T(s)\right)^{-1}\boldsymbol{\phi}_2(s)Q(e_i(s)) = \left(\boldsymbol{\phi}_2(s)\boldsymbol{\phi}_2^T(s)\right)^{-1}\boldsymbol{\phi}_2(s)e_i^2(s) \tag{4.31}$$

As long as $\boldsymbol{\phi}_2(s)\boldsymbol{\phi}_2^T(s)$ is invertible the parameter set $\boldsymbol{\theta}_{2_i}$ that minimizes $Q(e_i(t))$ has the least parameter error.

4.2.2 MME 2: Multiple Model Observer

A possible drawback of MME 1 is that the errors are obtained without using the dynamics of the model. The estimated output of each model, $\hat{y}_i$, are obtained from measured signals. This implies that the error at time k only depends on the parameters and the input signals at that time. If a dynamical model was used, the error would affect future errors and therefore make the differences between the models more apparent.

A step in this direction is running several observers in parallel and choose the parameter set that generates the least observer error[1]. This yields the errors

[1] This is referred to as Multiple Model Observer parameter estimation in [5].

$$e_i[k] = \dot{\psi}[k] - \dot{\hat{\psi}}[k] \tag{4.32}$$

where $\dot{\hat{\psi}}$ is the yaw rate calculated by the observer in (3.22). Intuitively, this approach makes sense in combination with the disturbance observer since the side wind estimate is based on the observer error. Therefore, parameters that minimize this when there is no side wind should provide a good side wind estimate. Figure 4.3 presents how the errors are obtained.

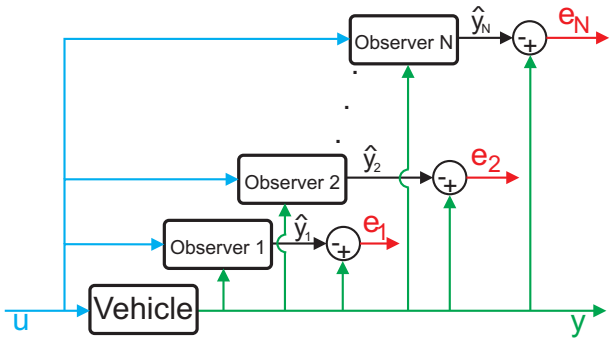

Figure 4.3: Sketch of how e_i are obtained using Multiple Model Observer parameter estimation

4.2.3 MME 3: Model Error

The third and final variation on how to obtain the error signals is to remove the observer term in MME2 and thus run N one-track models in parallel. If the initial conditions are correct, this MME should augment parameter error well since there is no corrective term. The errors are obtained according to the following equation.

$$e_i[k+1] = \dot{\psi}[k+1] - \widehat{\dot{\psi}}[k+1] = \dot{\psi}[k+1] - \Phi_d(\theta_i)\widehat{\dot{\psi}}[k] - \Gamma_d(\theta_i)u(\theta_i)[k] \tag{4.33}$$

where $\widehat{\dot{\psi}}$ indicates the yaw rate calculated by a vehicle model without observer term.

4.3 Implementation and Experimental Results

The proposed strategies for estimating C_r and C_f were implemented in Matlab/Simulink so that it was possible to apply them to measurement data. Different measurement sets were then used to evaluate the performance of the estimators.

4.3.1 Comparison of the MME Strategies

The three MME strategies were compared in terms of how well they converged. One topic which might be confusing regarding MME is how to decide if the algorithm has converged or not. Since the algorithm chooses from a pre-defined library, it can not be expected that the returned estimate is optimal among all possible values. When the algorithm returns the lowest (or the highest) value from the library it is likely that this is the case. It is then impossible to be certain if an even lower (or higher) value would yield a smaller error. In the experiments presented in this section, the lower (or upper) limit was adjusted whenever this occurred. In some cases, however, the limits had to be adjusted far beyond what is physically plausible and it was then decided that the estimation had failed.

Five different values of C_r and C_f were chosen, generating 25 combinations. Of the three estimators, MME1 performed the poorest since it only converged for a few measurements. The choice between MME2 and MME3 is dependent on the input to the estimators. When it consisted of large steering angles yielding large yaw rates, MME2 performed better, while MME3 was more suitable for more modest maneuvers. It is therefore likely that MME3 would be the best choice for normal driving.

The switching hysteresis also proved useful. Figure 4.4 displays the output of MME2 with and without hysteresis. The hysteresis removes the chattering and it may therefore be concluded that the errors connected with the parameter estimates in the region $[1.4, 1.55] \cdot 10^5$ are fairly equal.

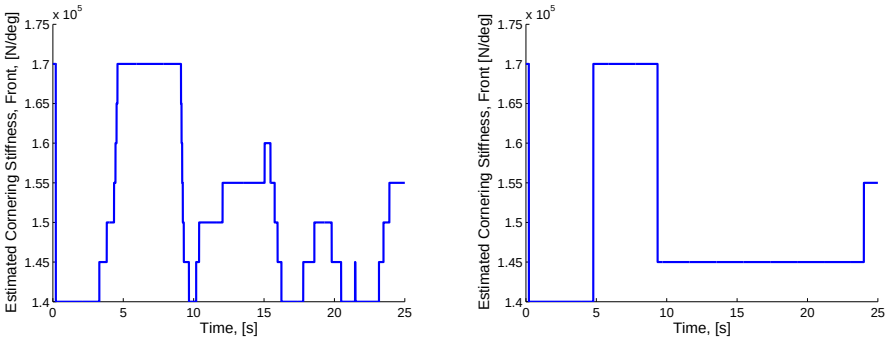

(a) Without hysteresis

(b) With a hysteresis of 0.03

Figure 4.4: The estimate of MME2 with and without switching hysteresis.

To make MME more convenient to use in different models and vehicles, MME2 and MME3 were implemented as Simulink libraries. The libraries accept up to 25 combinations of C_f and C_r and also have an input which pauses the estimation when its value is negative or zero. This input may typically be used to avoid estimating during heavy acceleration or deceler-

ation, since the vehicle model produces poor fit under these circumstances. The outputs are $\widehat{C}_r$ and $\widehat{C}_f$, the yaw rate of each model and their respective errors.

4.3.2 The Role of the Forgetting Factor in LS2

The choice of forgetting factor for recursive least squares plays an important role. In the following, LS2 will be applied to measurement data recorded at 80 km/h using a Mercedes S-class. The input signal consisted of steps in the steering wheel angle with a period of approximately 4 seconds. In Figure 4.5 the output of LS2 with $\lambda = 0.995$ and $\lambda = 0.999$ is presented. These values correspond to N_λ=200 and N_λ=1000 respectively. With a sample time of 0.005 seconds, this means that data recorded during the last second is used for the smaller value and data from the last five seconds for the larger.

For the smaller value of λ, the algorithm places the estimates in their correct regions but they are rather messy. A likely explanation for this is that the fit of the one-track model is poor during heavy turning. For instance, certain transients in the tyre forces have been disregarded yielding a small mismatch at each turn. When using the larger value, the estimates behave smoothly, since the averaging effect of a higher forgetting factor makes the estimates less sensitive to disturbances.

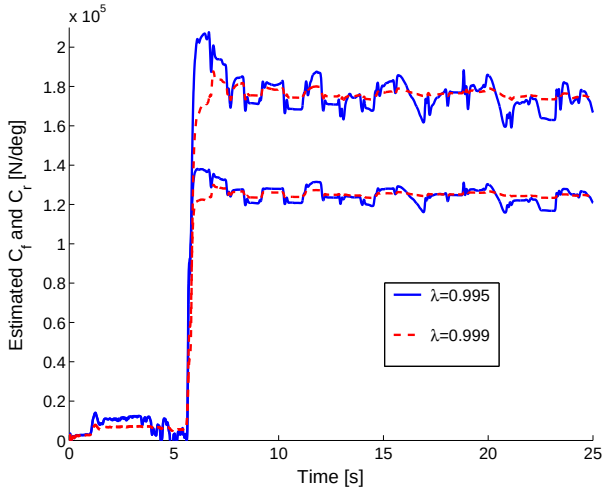

Figure 4.5: LS2 with $\lambda = 0.995$ and $\lambda = 0.999$.

The results of the original SVD-test and the two modifications proposed in Section 4.1.5 are displayed in Figure 4.6. As previously mentioned, the original svd-test states that two parameters may be identified regardless of the value of the forgetting factor. The modified tests are very restrictive

when the smaller value of λ is used. The second modification allows two parameters to be identified on two, very brief, occasions while the first modification remains at 1 through the whole measurement. When increasing the forgetting factor to 0.999, the first modification switches between one and two parameters but most of the time it states that two parameters may be identified. The estimation was not a complete failure for $\lambda = 0.995$ which indicates that the modifications produce somewhat conservative statements.

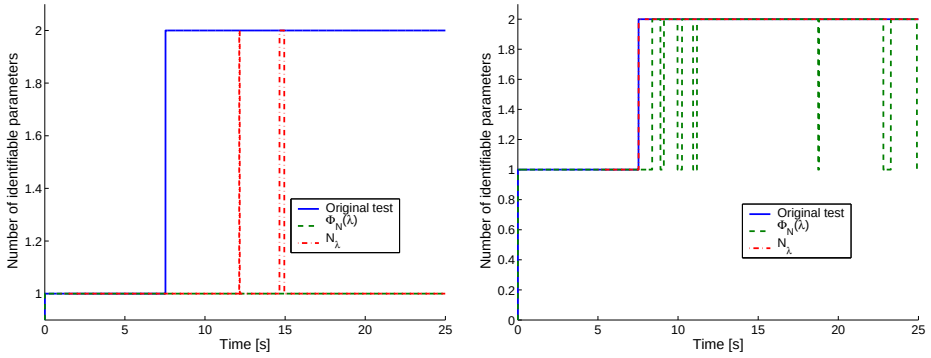

(a) $\lambda = 0.995$ (b) $\lambda = 0.999$

Figure 4.6: The number of identifiable parameters for two values of λ using the original svd-test and the two modifications proposed in Section 4.1.5.

4.3.3 Sensitivity to Sensor Offset

Both estimation methods are highly sensitive to sensor offset. Figure 4.7 (a) displays the measured lateral acceleration and the product $v_x\dot{\psi}$. According to Equation (2.8) these should be equal in stationary, i.e. when $\dot{v}_y = 0$. Figure 4.7 (b) shows the corresponding outputs of LS1 and MME3. Both methods fail to find the correct value of approximately 150 kN/deg.

Figure 4.8 displays the same plots as Figure 4.7 but the offset has been removed by requiring $a_y = v_x\dot{\psi}$ in stationary. This time, both methods converge to a value reasonably close to the actual. The difference between the two estimates is also much smaller than in Figure 4.7.

Clearly, it is necessary to remove any offsets present in the measured signals before attempting to estimate parameters. When doing this, one must be careful not to affect the results of the estimation. The criterion $a_y = v_x\dot{\psi}$ is not based on any assumption about the magnitudes of C_f and C_r. If the driving maneuver is symmetric around zero, it is sometimes possible to remove offsets by requiring that the mean value of the steering angle, yaw rate and lateral acceleration is zero. However, when considering the fit to a one-track model, values for C_r and C_f need to be specified. This may force the estimation into finding a specific value.

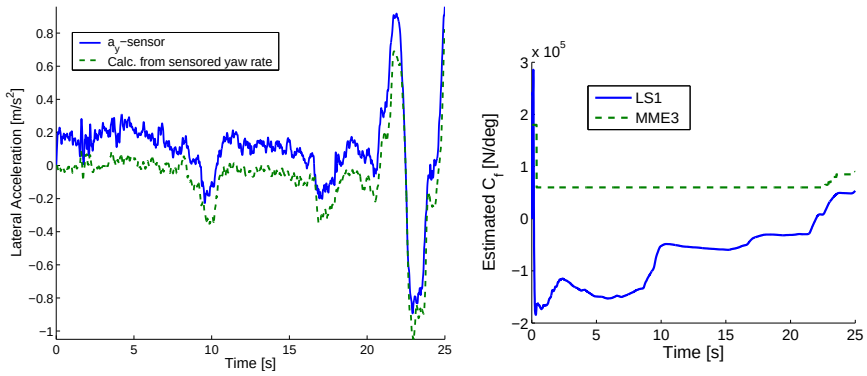

(a) a_y versus $v_x\dot{\psi}$ (b) Estimated C_f

Figure 4.7: Measured a_y versus $v_x\dot{\psi}$ and the estimates of LS1 and MME3.

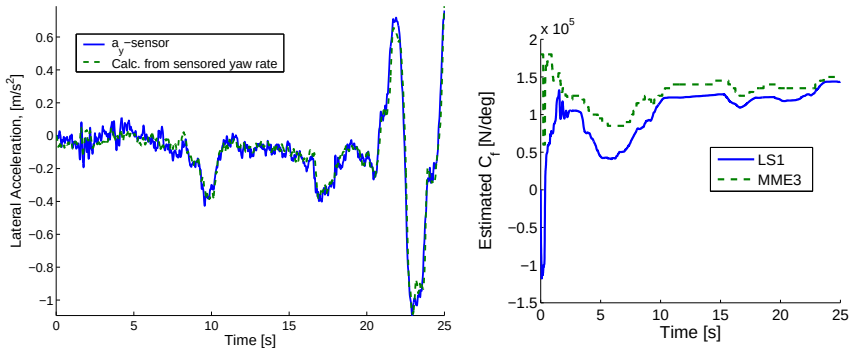

(a) a_y versus $v_x\dot{\psi}$ (b) Estimated C_f

Figure 4.8: Measured a_y versus $v_x\dot{\psi}$ and the estimates of LS1 and MME3.

4.3.4 Identification of Ordinary and Winter Tyres

In order to test the performance of the estimation strategies, Multiple Model Estimation and Recursive Least Squares were applied to measurements made with an S-class. The goal of this experiment was to investigate if it is possible to distinguish between ordinary tyres and winter tyres. Measurements were made with both tyre types at speeds around 80 km/h and 120 km/h. The steering input consisted of steps with somewhat varying period time and amplitude, a typical example is displayed in Figure 4.9.

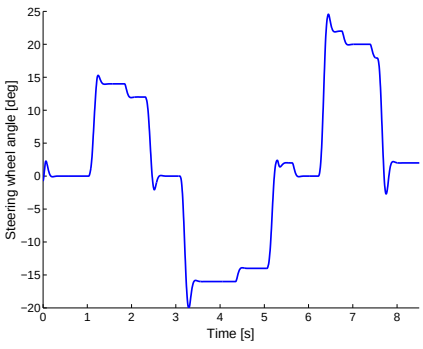

Figure 4.9: Steering input.

Three estimators were used; MME2, LS2, and LS2 with conditional updating, which will be referred to as LS2* in the following. The initial values where set to zero for the two least squares methods and $P[0]$ was set to 10^8 times the identity matrix. The forgetting factor was set to 0.999 for LS2 and to 0.996, which is substantially lower, for LS2*. It may then be investigated if the lower forgetting factor can yield a faster convergence without estimator windup. The estimate and covariance matrix were updated when the following condition was fulfilled, which allowed approximately half of the samples to be used.

$$\phi^T[t]P[t-1]\phi[t] > 1 - \lambda \tag{4.34}$$

The estimators were applied to four measurements for each tyre type. The results of the experiments are presented in Figures 4.11 and 4.12. Generally, the estimates of MME2 are somewhat higher than those of the least squares algorithms. The least squares estimates also vary more between the different measurements.

The use of conditional updating did not provide any major advantage over LS2. An example of the estimates of LS2 and LS2* is displayed in Figure 4.10. The figure displays the estimate $\hat{\boldsymbol{\theta}}$ and element (1,1) of the P-matrix. For LS2 with $\lambda = 0.996$, the rather large peaks in the lower plot indicate that estimator windup occurred. The peaks are attenuated when using LS2* and the estimates behave more smoothly. Increasing the forgetting factor for LS2 decreases the peaks even further with a only a small increase in convergence time. All three estimators are fairly consistent after approximately 15 seconds.

When studying the spread of the estimates in Figure 4.11 it is clear that the estimate of C_f varies more for ordinary tyres than for winter tyres. A plausible explanation for this is that the maneuvers performed with the ordinary tyres varied more. In some of the measurements rather large steering angles were applied, violating the assumption of small slip angles and thus affecting the estimated cornering stiffness. The principle of this effect is presented in Figure 4.13, where the initial slope of the curve is the actual value of C_f. When the slip angles are large, the curve turns nonlinear. The estimators, however, are designed under the assumption of a linear relation between slip angle and tyre force, which results in an estimate that is too small.

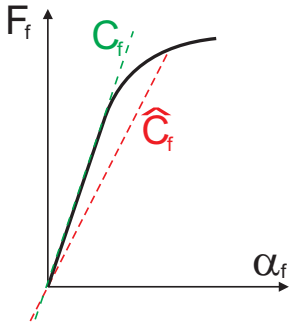

Figure 4.13: Falsely estimated cornering stiffness.

Taking the mean value of all estimates for each tyre type yields that C_r is

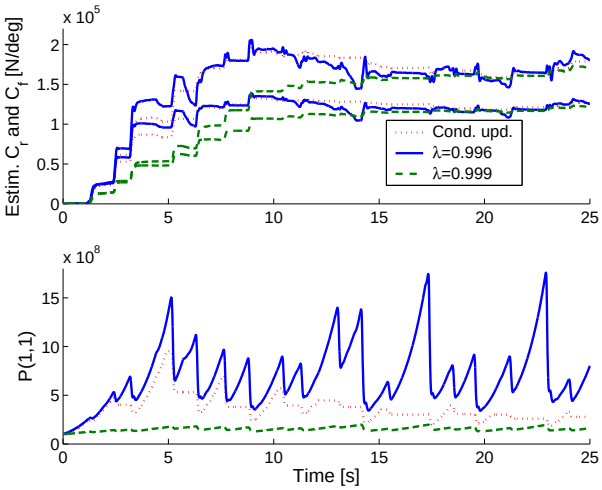

Figure 4.10: The estimate and element (1,1) of the covariance matrix P for LS2 with $\lambda = 0.996$, LS2 with $\lambda = 0.999$, and LS2* with $\lambda = 0.996$ (denoted Cond. upd.).

178 kN/deg for normal tyres and approximately 141 kN/deg for winter tyres. The corresponding values for C_f are approximately 123 and 117 kN/deg. For ordinary tyres, C_r and C_f have been found to be approximately 170 and 120 kN/deg respectively. The results of the estimation are consistent with this and the magnitude of the decrease in cornering stiffness when using winter tyres is plausible. This experiment is therefore a strong indication that cornering stiffness can be identified by the use of MME or LS. However, as previously mentioned, sensor offset needs to be removed from the signals before any successful parameter identifications can be made. In order to use MME it is also necessary to have some a priori information regarding in which regions C_r and C_f can be expected to lie.

4.4 Aerodynamic Effects

In this Section, the effects of aerodynamic drag and aerodynamic lift on the cornering stiffness will be investigated, using a few results from Sections 2.2 and 2.5. It should be noted that no systematic difference between the estimates at 80 km/h and 120 km/h was distinguishable in Section 4.3.4. A previous investigation of aerodynamic effects is presented in [11]. For further reading on the aerodynamics of vehicles, see [4].

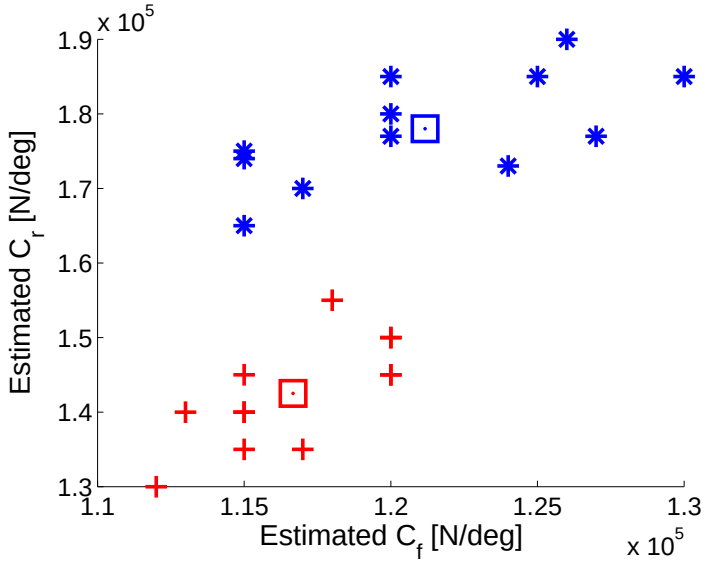

Figure 4.11: Estimation results for the measurements with ordinary (blue $*$) and winter (red $+$) tyres. The mean value for each tyre type is marked with a square.

4.4.1 Aerodynamic Drag

Consider Figure 4.14 where aerodynamic drag $F_{w,x}$, aerodynamics lift $F_{w,z}$ and the longitudinal tyre force, $F_{l,r}$, are presented. The aerodynamic drag when driving straight ahead is given by Equation (2.23) with $\tau_{air} = 0$.

$$F_{w,x} = \frac{1}{2}\rho_{air} c_{air,x}(0) A_{air} \boldsymbol{v}^2 \tag{4.35}$$

The longitudinal tyre force must compensate for $F_{w,x}$ and the rolling resistance of the tyre, F_R, which gives the following expression.

$$F_{l,r} = \frac{1}{2}\rho_{air} c_{air}(0) A_{air} \boldsymbol{v}^2 + F_R \tag{4.36}$$

By making use of Equation (2.42), which states that $F_l \approx C_l \lambda$, the slip is obtained as a function of velocity.

$$\lambda \approx \frac{1}{C_l}\left(\frac{1}{2}\rho_{air} c_{air} A_{air} \boldsymbol{v}^2 + F_R\right) \tag{4.37}$$

The lateral force on the rear tyre F_r is then given by

$$F_r = F_{z,r}\mu(\lambda) \tag{4.38}$$

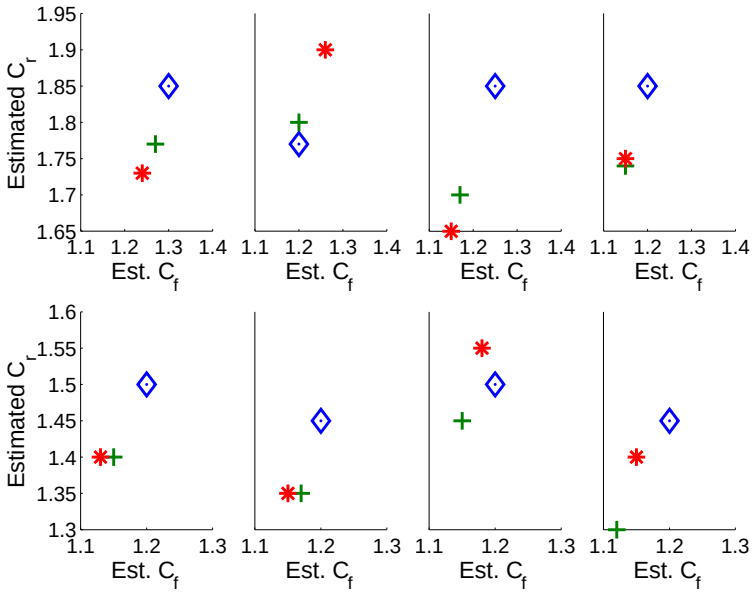

Figure 4.12: Estimation results for each measurement. The upper row correspond to ordinary tyres while the lower corresponds to winter tyres. MME is marked with $\diamond$, LS2 with $+$ and LS2* with $*$. The values are plotted in factors of 10^5 N/deg.

The load force on the rear tyre, $F_{z,r}$, is given by a moment equation around the front wheel.

$$F_{z,r} = -\frac{mgl_f}{L}$$

The function $\mu(\lambda)$ may now be calculated with a tyre model which has been implemented in Matlab at DaimlerChrysler. It takes $F_{z,r}$, λ and α_r as inputs and outputs F_r. By evaluating the initial slope when F_r is plotted against α_r a value for C_r is found. Repeating the procedure with different values of

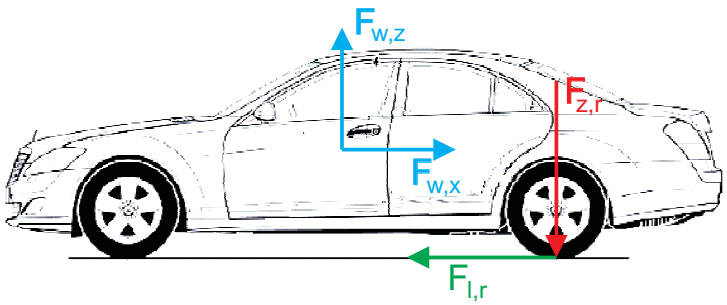

Figure 4.14: The aerodynamic forces $F_{w,x}$ and $F_{w,z}$.

v [km/h]	50	100	150	200
C_r (drag)	8.7563	8.7569	8.7608	8.7207
C_r (drag & lift)	8.7353	8.6727	8.5712	8.3866

Table 4.1: Calculated C_r from aerodynamic effects for various speeds. The values of C_r are given in factors of 10^4 N/deg.

$\boldsymbol{v}$ gives an indication on how lateral drag affects the cornering stiffness at high speeds.

4.4.2 Aerodynamic Lift

The aerodynamic forces also create a lift force acting according to

$$F_{w,z} = \frac{1}{2}\rho_{air} c_{air}(0) A_{air} \boldsymbol{v}^2 \tag{4.39}$$

This will reduce the resulting force on the rear tyre in the following way.

$$F_{z,r} = -\frac{mgl_f}{L} + \frac{F_{w,z}}{2}$$

With an altered $F_{z,r}$ the quotient between F_r and α_r is altered and therefore correspond to a different value of C_r, which may be calculated in the same way as in the previous section.

4.4.3 Simulation Results

The calculated stiffness of the rear tyre for various speeds is presented in Table 4.1. The calculations based on aerodynamic drag yield a decrease of C_r of 0.41 % as the speed increases from 50 km/h to 200 km/h. When also considering aerodynamic lift the decrease is 3.99 % for the same speeds. The simulations imply that aerodynamic lift has a larger impact on tyre stiffness than aerodynamic drag. Both effects are, however, rather small.

Chapter 5

Closing the Loop

The main objective with estimating side wind is to attenuate it in order to assist the driver. A controller will be designed and evaluated in terms of how well it keeps the yaw rate down during side wind.

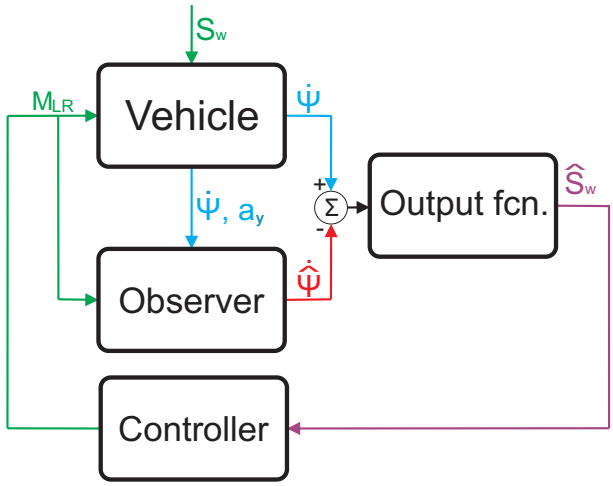

Figure 5.1: Principle of the side wind attenuation.

5.1 The EPS-actuator

The side wind is to be suppressed using Electric Power Steering (EPS). EPS applies a torque on the steering rod, and thus turns the steering wheel. This means that it is possible for the driver to counteract the controller by holding the steering wheel straight. It also means that the applied torque can not be too strong, as it most likely would be frightening for the driver if the steering

wheel turned too fast on its own.

5.2 Controller Design

To attenuate side wind acting on the vehicle, the estimate is passed to a controller which acts on the moment actuator on the steering rod, see Figure 5.1. A fairly common way of canceling the effects of known disturbances is feedforward compensation, which is described in [7].

5.2.1 Feedforward Compensation

Assume that a system with transfer function $G(s)$, input u, and output y is affected by a disturbance v, and that this disturbance may be measured. A controller is implemented according to Figure 5.2, where G_{ff} is to be chosen. If the transfer function from v to y, $G_v(s)$, is known and $G(s)$ has a stable and realizable inverse, the disturbance is canceled by use of the control signal $u(s) = G_{ff}(s)v(s) = -G^{-1}(s)G_v(s)v(s)$.

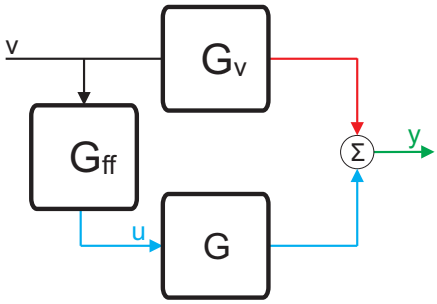

Figure 5.2: Feedforward control.

When this is impossible, a pragmatic solution is to calculate, or approximate, the steady state gain, which might perform well enough in many cases. Another reason for choosing to disregard the dynamics is that the model generally produces better fit at lower frequencies. In the following, a stationary feedforward gain will be calculated.

To calculate the torque needed to compensate for a certain, stationary, side wind, the second-order vehicle model derived in Chapter 2, i.e. the matrices in (2.32), will be used. However, the G-matrix will be modified into G_{ctrl} by discarding the first column so that side wind is the only disturbance entering the system. In stationary, the state vector is

$$\boldsymbol{x}_\infty = \begin{pmatrix} v_{y\infty} \\ \dot{\psi}_\infty \end{pmatrix} = -A^{-1}B\delta_\infty - A^{-1}G_{ctrl}S_{w_\infty} \tag{5.1}$$

The inverse of A is

$$A^{-1} = \frac{Jmv_{x_\infty}}{L^2C_fC_r + m\rho v_{x_\infty}} \begin{pmatrix} -\frac{\kappa}{J} & v_{x_\infty}^2 - \frac{\rho}{m} \\ -\frac{\rho}{J} & -\frac{\sigma}{m} \end{pmatrix} \tag{5.2}$$

The products $A^{-1}B$ and $A^{-1}G_{ctrl}$ may then be calculated

$$A^{-1}B = \frac{v_{x_\infty}}{L^2C_fC_r + m\rho v_{x_\infty}^2} \begin{pmatrix} l_fC_fmv_{x_\infty}^2 - Ll_rC_fC_r \\ -LC_fC_r \end{pmatrix} \tag{5.3}$$

$$A^{-1}G_{ctrl} = \frac{v_{x_\infty}}{L^2C_fC_r + m\rho v_{x_\infty}^2} \begin{pmatrix} -\kappa + emv_{x_\infty}^2 - \rho e \\ -\rho - \sigma e \end{pmatrix} \tag{5.4}$$

This yields the following equations for the stationary lateral velocity and yaw rate.

$$\frac{v_{y_\infty}}{v_{x_\infty}} = \xi^{-1}\Big(\left(l_fC_fmv_{x_\infty}^2 - Ll_rC_fC_r\right)\delta_\infty + \left(-\kappa + emv_{x_\infty}^2 - \rho e\right)S_{w_\infty}\Big) \tag{5.5}$$

$$\dot{\psi}_\infty = v_{x_\infty}\xi^{-1}\Big(- LC_fC_r\delta_\infty - (\rho + \sigma e)S_{w_\infty}\Big) \tag{5.6}$$

where $\xi = L^2C_fC_r + m\rho v_{x_\infty}^2$.

Setting $\dot{\psi}_\infty = 0$ and solving (5.6) for δ_∞ yields the following control law for δ_∞.

$$\delta_\infty = -\frac{\rho + \sigma e}{LC_fC_r}S_{w_\infty} \tag{5.7}$$

By inserting this expression into (5.5) an expression for lateral velocity as a function of longitudinal velocity and side wind is obtained.

$$\frac{v_{y_\infty}}{v_{x_\infty}} = \xi^{-1}\Big(\left(l_fC_fmv_{x_\infty}^2 - Ll_rC_fC_r\right)\frac{\rho + \sigma e}{LC_fC_r} - \kappa + emv_{x_\infty}^2 - \rho e\Big)S_{w_\infty} \tag{5.8}$$

To calculate the stationary moment needed to obtain a certain steering angle, (2.44) is used. In stationary, it becomes

$$M_{LR_\infty} = \frac{1}{i_L}\left(C_M\left(i_L\delta_\infty - \delta_{LR_\infty}\right) + n_kC_f\left(\delta_\infty - \frac{v_{y_\infty}}{v_{x_\infty}} - \frac{l_f}{v_{x_\infty}}\dot{\psi}_\infty\right)\right) \tag{5.9}$$

Since $\dot{\psi}_\infty$ has been set to zero, (5.7) and (5.8) may be inserted into (5.9) which yields the following stationary moment.

$$M_{LR_\infty} = \frac{1}{i_L}\Bigg(- c_M\delta_{LR_\infty} + \Bigg(- (c_M i_L + n_k C_f)\frac{\rho+\sigma e}{LC_fC_r} - \\ n_k C_f \xi^{-1}\Bigg(\left(l_f C_f m v_{x_\infty}^2 - L l_r C_f C_r\right)\frac{\rho+\sigma e}{LC_fC_r} - \kappa + e m v_{x_\infty}^2 - \rho e\Bigg)\Bigg) S_{w_\infty}\Bigg) \tag{5.10}$$

To obtain a faster response to changes in side wind, a derivative part will be added, which yields the following, dynamical, control law.

$$M_{LR}(t) = K_p M_{LR_\infty}(t) + K_d \frac{\partial}{\partial t} M_{LR_\infty}(t) \tag{5.11}$$

where $M_{LR_\infty}(t)$ denotes the moment calculated according to (5.10) with $\delta_{LR}(t)$, $\widehat{S}_w(t)$ and $v_x(t)$ as inputs. The design parameters are the two gains K_p and K_d. Since $M_{LR_\infty}(t)$ should provide all the stationary gain needed to suppress the disturbance, K_p is set to one and only K_d needs to be tuned using simulations or real life tests.

5.2.2 Tuning the Controller

CASCaDE was used to simulate a vehicle driving past side wind in order to tune K_d. Since a few dynamics of the steering system were left out when deriving the model, it was also necessary to tune K_p somewhat.

Figure 5.3 displays the yaw rate and applied moment for a few values of K_p. The results when $K_d = K_p = 0$ is also displayed. In this case, the yaw rate has a negative slope during the side wind. This is caused by the vehicles rotation away from the side wind, which makes the lateral force smaller. The vehicle velocity was set to 130 km/h and the wind velocity to 54 km/h. As expected, the controller keeps the yaw rate close to zero for all values of K_d. The initial peaks are reduced by choosing a higher value, but the applied moment is almost doubled when K_d is increased from 0.1 to 0.5. The choice of K_d therefore needs to be made in a real vehicle where the comfort of the driver and passengers may be evaluated for the different values.

5.2.3 Limiting the Controller

The fact that the controller is to be used in a car introduces a few special issues. One situation which may result in an unpleasant experience for the driver is if the moment suddenly disappears. One possible solution to this is to let the applied moment disappear slowly once the side wind is stationary

and then leave the compensation to the driver. When a side wind hits the vehicle, the controller turns the steering wheel to an appropriate angle and then lets the driver take over. There are several ways of obtaining this. One is to pass the estimated side wind through a high-pass filter and thus remove any stationary control action. A positive side effect of this strategy is that it also removes the effects of sensor offset.

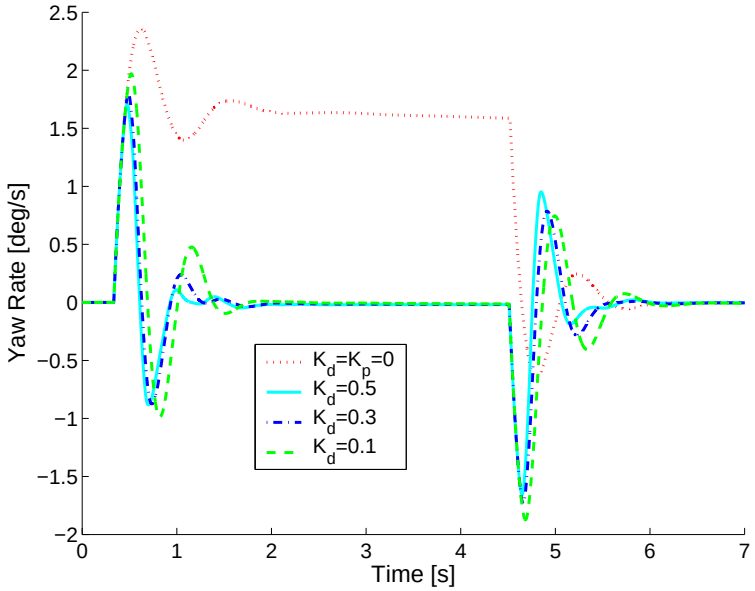

(a) $\dot{\psi}$

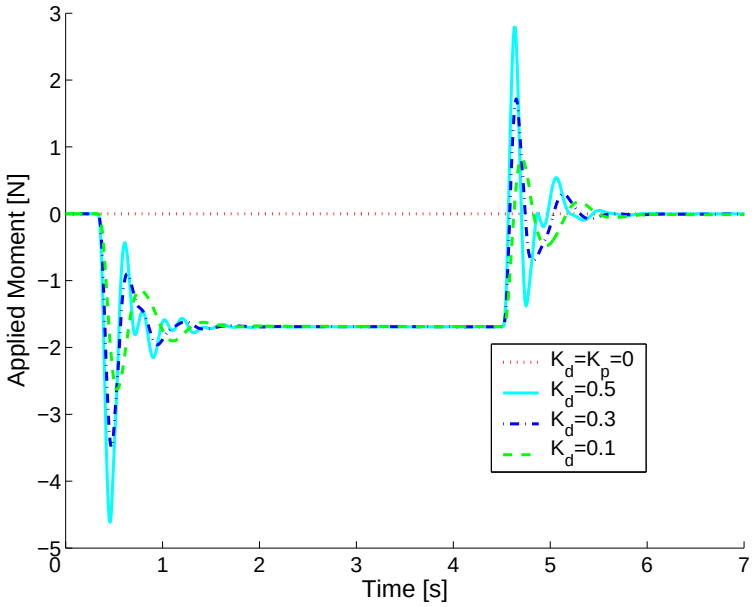

(b) M_{LR}

Figure 5.3: The yaw rate and the applied moment with $v = 130$ km/h and a side wind of 15 m/s.

Chapter 6

Conclusions and Future Work

6.1 Conclusions

This work was focused on the estimation of side wind using a first-order disturbance observer. The robustness towards sensor offset and parameter error have been investigated. A few possibilities for reducing the effects of sensor offset have been presented. To improve on the sensitivity to parameter error, Recursive Least Squares and Multiple Model Estimation were applied in order to identify the cornering stiffness of the tyres. Both methods were found capable of distinguishing between ordinary tyres and winter tyres. A feedforward controller was designed which uses the side wind estimate to assist the driver during wind gusts.

6.2 Future Work

Several issues remain regarding the on line identification. A major issue is that of deciding when to perform identification. One criterion is to run the identification at lower speeds and estimate side wind at higher. At winter time, however, it is not unlikely that the driver starts on snow or ice and then enters a snow-free motorway. The estimated parameters will then be inaccurate. It would also be desirable to develop further criteria for determining if the identification was successful or not. Two procedures which uses singular value decomposition of the regressor matrix have been proposed, which need to be investigated further. It might also be possible to improve the identification by using a more complex vehicle model, e.g. by introducing the dynamics of the steering system and those of the tyre forces.

Bibliography

[1] Jens Kalkkuhl, Christian Urban
Ein Erweitertes Kalmanfilter zur Seitenwinddetektion
Technischer Bericht, DaimlerChrysler, 2005

[2] A. Alcocer, A. Robertsson, A. Valera, R. Johansson
Force Estimation and Control in Robot Manipulators
Conference Paper, 7th Symposium on Robot Control, 2003

[3] A. Alcocer
Force Estimation and Control in vehicles and robots
Master's Thesis, Dept. Automatic Control, Lund Institute of Technology, 2002

[4] M. Mitschke, H. Wallentowitz
Dynamik der Kraftfahrzeuge
Springer, Berlin, 2004

[5] Jens Lüdemann
Heterogeneous and Hybrid Control with Application in Automotive Systems
Dissertation, Glasgow University, 2002

[6] Dieter Ammon
Modellbildung und Systementwicklung in der Fahrzeugdynamik
Teubner Verlag, 1997

[7] Karl J. Åström, Björn Wittenmark
Computer Controlled Systems - 3rd ed.
Prentice-Hall Inc., 1997

[8] Karl J. Åström, Björn Wittenmark
Adaptive Control - 2nd ed.
Addison-Wesley Publishing Company, 1995

[9] Rolf Johansson
System Modeling & Identification - 2nd ed.
Prentice Hall, Eaglewood Cliffs, 2006

[10] Erich Schindler
Vehicle Dynamics
Lecture Notes, FHTE Esslingen, University of Applied Sciences

[11] Christian Ludwig
Qualifikation von Fahrverhaltensmodellen für hohe Geschwindigkeiten
Master's Thesis, Fachhochschule Esslingen, 2003

[12] Gene H. Golub, Charles F. van Loan
Matrix Computations - 2nd ed.
The John Hopkins University Press, 1989

[13] J.P. Hespanha
Logic-Based Switching Algorithms in Control
Dissertation, Graduate School, Yale University, 1998

[14] Zoltán Á. Zomotor
Online-Identifikation der Fahrdynamik zur Bewertung des Fahrverhaltens von Pkw
Dissertation, Institut A für Mechanik, Stuttgart University, 2002